SOUNDING ROCKET PERFORMANCE ANALYSIS

Thesis

by

James D. Burke

In Partial Fulfillment of the Requirements

For the Degree of

Aeronautical Engineer

California Institute of Technology

Pasadena, California

1949

ACKNOWLEDGEMENTS

The author is deeply grateful to Mr. Henry T. Nagamatsu for his advice and encouragement in the preparation of this thesis, and to Dr. Clark B. Millikan for his generous assistance in the selection of subject and initiation of the work.

ABSTRACT

An investigation of the effects of basic design parameters on the performance of a single-stage sounding rocket was made. The tail area required for static stability at various supersonic flight Mach numbers was determined, and the drag coefficient for various configurations was calculated. The general equations of motion for flight in vacuum were integrated for several cases to show the effect of varying specific impulse of fuel, propellant weight ratio, and burning time. An approximate solution of the equations for trajectories in air was obtained by the method of stepwise numerical integration.

TABLE OF CONTENTS

I. INTRODUCTION

One of the most interesting peacetime applications of rocket propulsion is the vertical sounding rocket, used as a vehicle for carrying instruments and cameras to extreme altitudes.

Recent developments, highlighted by the 251-mile ascension of an A-4 Bumper Wac two stage rocket from White Sands, make the study of sounding rocket performance an attractive research project.

The purpose of the present investigation was to evaluate in detail the influence of certain design parameters upon the vertical trajectory of a sounding rocket, and to consider not only the presently attainable values of these parameters, but also a few cases illustrating what may be possible in future development.

The analysis of sounding rocket trajectories has been carried out by numerous authors, in many instances with special reference to the limiting case of the "escape rocket" which departs from the gravitational field of the Earth. The papers of most immediate interest in the present investigation were those of Malina and Smith (Ref. 1), Tsien and Malina (Ref. 2), and Siefert, Mills, and Summerfield (Ref. 3). The latter gives, in addition to a discussion of the equations and parameters involved, a brief history and bibliography of high-altitude rocket development.

In the analysis presented in this Thesis, it was found advisable to assume a basic configuration for the rocket, and then to calculate the size of the tail fins required to stabilize

the vehicle at the highest Mach number expected during flight. With these tail areas the overall drag coefficient was determined, and finally the performance of the rocket was ascertained by numerical step-by-step integration of the equations of motion. In this Thesis, Section III deals with the aerodynamic calculations for static stability and drag coefficient. Section IV discusses the equations of motion and the parameters to be studied, and shows the influence of these parameters upon the performance in vacuum. Section V is concerned with the numerical calculations for the trajectory in the NACA standard atmosphere, and Section VI presents the conclusions.

II. LIST OF NOTATION

C_L	Lift Coefficient
α	Angle of attack, radians
L	Lift
A	Cross sectional area of rocket body
ρ	Air density
V	Flight velocity
q	Dynamic pressure $= \frac{1}{2}\rho V^2$
d	Diameter of rocket body
S_T	Planform area of two tail fins
$()_B$	refers to body without fins
$()_T$	refers to tail fins
V_S	Velocity of sound
M	Mach number of flight, V/V_S
$()_M$	refers to conditions at Mach number M
$()_{M=0}$	refers to incompressible case
$l_{C\alpha}$, l_B, l_T, l_{CP}, C_0	Defined in Fig. 2
C_m	Pitching moment coefficient
$()_N$	refers to conditions on conical nose
θ_S	cone semivertex angle, degrees
C_f	Local skin friction drag coefficient
D_f	Drag due to friction
S	Wetted area of body excepting area of base

List of Notation (cont.)

C_{D_F} Overall body skin friction drag coefficient

P_B Base pressure coefficient

p_B Pressure acting over base

C_{D_B} Base pressure drag coefficient

C_{D_1} Total body drag coefficient

$C_{D_{\pi_W}}$ Section wave drag coefficient

$C_{D_{\pi F}}$ Section skin friction drag coefficient

C_{D_π} Total tail drag coefficient based on S_T

C_{D_T} Total tail drag coefficient based on d^2

C_D Total drag coefficient for complete rocket

F Thrust, lb.

D Drag, lb.

W Weight, lb.

g Acceleration of gravity, ft/sec^2

t Time, sec.

W_F Weight of propellant

ν Propellant weight ratio, $\frac{W_F}{W_o}$

$()_p$ refers to conditions at end of burning

I Specific impulse of propellant, lb sec/lb

σ Air density ratio $= \rho/\rho_o$

μ Loading factor $= \frac{W_o}{d^2}$

y Altitude above Earth's surface, ft.

y_s Altitude at summit of trajectory

List of Notation (cont.)

y_c Altitude gained due to coasting after burnout

$()_o$ refers to conditions at Earth's surface

R Radius of the Earth

$()_g$ refers to quantities corrected for variation of gravity with altitude

III. STATIC STABILITY AND DRAG ANALYSIS

A. Determination of Tail Area Required for Static Stability at Various Mach Numbers

It is known from experiment that the aerodynamic center of pressure on a slender fin-stabilized rocket moves forward as the Mach number of flight is increased; therefore, the greater the design Mach number, the larger the tail area required for static longitudinal stability. In this study we have considered a family of rockets, all having the same body dimensions, with fins of similar shape but varying size. (Cf. Fig. (1)).

Lift of Body

The flow about bodies of revolution at both subsonic and supersonic speeds has been investigated by several authors; Tsien (Ref. 4) determines the lift coefficient for a conical body as a function of Mach number, cone angle, and angle of attack; Laitone (Ref. 5) uses a linearized theory to obtain a simple expression for $\frac{dC_L}{d\alpha}$ which shows some agreement with experiment. For a slender cone the slope of the lift curve for the body, based on linearized theory, is

$$\frac{dC_L}{d\alpha} = 2 ,$$

where C_L is defined as

$$C_L = \frac{L}{q_\infty A}$$

in which $A = \frac{\pi}{4} d^2$ is the cross-sectional area of the body.

In the present study it was found convenient to define dimensionless coefficients in terms of d^2 ; e. g.,

$$C_{L_B} = \frac{L_B}{q d^2}$$

and thus, the linearized slope of the lift curve is

$$\left(\frac{dC_L}{d\alpha}\right)_B = \frac{\pi}{2} = 1.57$$

For a long slender body at supersonic Mach numbers, however, it is found that $\left(\frac{dC_L}{d\alpha}\right)_B$ is considerably larger than this value; a plot of estimated values versus Mach number is given in Fig. (4). At subsonic speeds the lift of the body is so small in comparison with that of the fins that it can safely be neglected in the determination of the total lift coefficient.

Lift of Fins

The section lift coefficient, $C_{L_{T\pi}}$, for the tail fins is defined as

$$C_{L_{T\pi}} = \frac{L_T}{q S_T}$$

Wienig (Ref. 6) gives observed and calculated values of the lift coefficient for wings of small aspect ratio in incompressible flow. For our fins we assumed $\left(\frac{dC_L}{d\alpha}\right)_{T\pi} = 1.4$, in the incompressible case, and applied the Prandtl-Glauert compressibility correction

$$\left(\frac{dC_L}{d\alpha}\right)_M = \frac{1}{\sqrt{1-M^2}} \left(\frac{dC_L}{d\alpha}\right)_{M=0}$$

to obtain $\left(\frac{dC_L}{d\alpha}\right)_{T\pi}$ as a function of Mach number in the subsonic range.

At supersonic speeds, the section lift coefficient for a thin airfoil may be calculated using Ackeret's small-perturbation theory (Ref. 7).

For a symmetrical biconvex circular arc airfoil, the section lift coefficient is given as

$$C_{L_{T_{TT}}} = \frac{4\alpha}{\sqrt{M^2-1}}$$

Hence,

$$\left(\frac{dC_L}{d\alpha}\right)_{T_{TT}} = \frac{4}{\sqrt{M^2-1}}$$

In Fig. (5), $\left(\frac{dC_L}{d\alpha}\right)_{T_{TT}}$ is plotted as a function of Mach number. It will be noted that since the linearized theories do not hold in the transonic range, it is necessary to estimate the values near $M = 1.0$. The same condition will be found in the curves of drag coefficient vs. Mach number. The errors in the estimation, however, have little effect on performance, since in most cases of interest the rocket accelerates rapidly through the transonic range.

Experimental results indicate that it is possible at supersonic speeds to neglect finite span and interference effects in determining the lift of rocket tail surfaces. If this is done, the tail lift coefficient, C_{L_T}, defined as

$$C_{L_T} = \frac{L_T}{q d^2}$$

may be written as

$$C_{L_T} = (C_{L_{T_{TT}}}) \frac{S_T}{d^2}$$

Thus,

$$\left(\frac{dC_L}{d\alpha}\right)_T = \left(\frac{dC_L}{d\alpha}\right)_{T_{TT}} \cdot \frac{S_T}{d^2}$$

The curves of $\left(\frac{dC_L}{d\alpha}\right)$ for the complete rocket as a function of Mach number with various tail areas are given in Fig. (6).

Fin Area Required for Static Stability

The determination of the fin area required for stability at various Mach numbers and of the center of pressure travel with Mach number for a given fin area was done under the following assumptions: (Cf. Fig. (2))

(1) The distance, l_{CG}, from the base, which is taken as the origin of moments, to the center of gravity is assumed constant and equal to 45% of the overall length, l_B. In dimensionless form, $\frac{l_{CG}}{d} = 0.45 \frac{l_B}{d} = 6.3$.

(2) The limit of stability is defined as the condition at which the center of pressure is one caliber aft of the assumed center of gravity; i. e., we have a one-caliber "margin of safety". At the limit of stability, $\frac{l_{CP}}{d} = 5.3$

(3) The lift of the tail, L_T, is assumed to act at 55% of the mean aerodynamic chord, measured from the trailing edge. This makes $l_T = 0.413\, C_o$, where C_o is the root chord of the tail fin.

(4) The lift of the body is assumed to act at the nose, $\frac{l_B}{d} = 14.0$. Tsien (Ref. 4) shows that the lift distribution for a long body gives a resultant lift vector near the nose. The assumption that the resultant vector is at the nose gives a slightly conservative result in most cases.

By taking the moments about the base of the rocket, we obtain

$$\frac{l_{CP}}{d} = \frac{\left(\frac{\partial C_m}{\partial \alpha}\right)}{\left(\frac{\partial C_L}{\partial \alpha}\right)}$$

where

$$\left(\frac{\partial C_m}{\partial \alpha}\right) = \left(\frac{\partial C_L}{\partial \alpha}\right)_B \frac{l_B}{d} + \left(\frac{\partial C_L}{\partial \alpha}\right)_T \frac{l_T}{d}$$

and

$$\left(\frac{\partial C_L}{\partial \alpha}\right) = \left(\frac{\partial C_L}{\partial \alpha}\right)_B + \left(\frac{\partial C_L}{\partial \alpha}\right)_T$$

Introducing the quantity $\left(\frac{\partial C_L}{\partial \alpha}\right)_{T\pi}$, we have

$$\frac{l_{CP}}{d} = \frac{\left(\frac{\partial C_L}{\partial \alpha}\right)_B \frac{l_B}{d} + \left(\frac{\partial C_L}{\partial \alpha}\right)_{T\pi} \frac{S_T l_T}{d^3}}{\left(\frac{\partial C_L}{\partial \alpha}\right)_B + \left(\frac{\partial C_L}{\partial \alpha}\right)_{T\pi} \frac{S_T}{d^2}}$$

Inserting numerical values for the limit of stability, $\frac{l_{CP}}{d} = 5.3$ and for S_T and l_T in terms of C_o, the fin root chord, the equation becomes

$$0.0115\left(\frac{\partial C_L}{\partial \alpha}\right)_{T\pi} C_o^3 - 0.4415\left(\frac{\partial C_L}{\partial \alpha}\right)_{T\pi} C_o^2 + 8.7\left(\frac{\partial C_L}{\partial \alpha}\right)_B = 0 .$$

By using the values of the coefficients from Figs. (4) and (5), this equation can be solved for C_o at any Mach number.

Fig. (7) gives a plot of tail fin area required for static stability as a function of Mach number, and Fig. (8) illustrates the location of center of pressure as a function of Mach number for various tail areas.

B. Determination of Drag Coefficient as a Function of Mach Number

Drag of the Body

The drag of a slender body traveling at supersonic speed has been investigated both experimentally and theoretically (Refs. 8, 9, and 10), and it is found that the total drag can be conveniently broken down into three parts: (1) the integrated pressure force due to formation of shock waves at the nose, here referred to as the "nose pressure drag"; (2) the total retarding force due to skin friction over the entire body; and (3) the drag resulting from reduced pressure operating over the base of the rocket, which we shall call the "base

pressure drag". In the case which we have studied, the nose pressure drag may be calculated directly, since an exact solution of the hydrodynamic equations is known. The skin friction and base pressure drag, on the other hand, are determined primarily by viscous flow conditions in the boundary layer about the body, and consequently, their exact determination is difficult, especially since no complete theory exists at present for boundary layers in supersonic flow.

It will be shown, however, that small errors in determination of the drag coefficient do not appreciably affect the ultimate performance. In the case of the skin friction it is justifiable to assume a constant average value consistent with the experimental data. The base pressure drag may be evaluated experimentally; the procedure is to measure the total drag, and then to estimate and subtract out the portions due to nose pressure and skin friction (Refs. 8 and 9). This procedure is necessarily susceptible to errors. Dean Chapman (Ref. 10) has presented an approximate theory for the determination of base pressure which gives satisfactory agreement with experiment; however, application of the theory to this case would be an unjustified refinement in view of the order of our approximation to the skin friction.

In accordance with these considerations, the base pressure drag coefficient used in this study was calculated from base pressure coefficient values estimated with the aid of Fig. 1, Ref. 10, which compares experimental results with the values predicted by various theories. The extrapolation of base pressure coefficient to high Mach numbers is not critical, since even at the relatively low

supersonic Mach number of 4.0 the base pressure drag is only about one tenth of the drag for the complete rocket. (Cf. Figs. (9) and (11)). By the same reasoning we can say that the influence on total drag of the propulsive jet issuing from the base of the rocket is small, even though the drag as we have determined it is strictly correct only for the case when the jet is absent.

The nose pressure drag coefficient, C_{D_N}, may be expressed as

$$C_{D_N} = \frac{D_N}{q d^2} = \frac{\pi}{2} \frac{(p_N - p)}{\rho V^2}$$

where the quantities are as defined in Fig. (3).
Using the tables of values of $\frac{p_N}{p}$ given by Z. Kopal (Ref. 11) for a cone semivertex angle, θ_S, of 7.5°, we obtained C_{D_N} as a function of Mach number.

The local skin friction drag coefficient, C_F, as defined by Karman and Moore (Ref. 8), is

$$C_F = \frac{D_F}{q S}$$

where D_F is the total drag due to friction and S is the wetted area of the body excepting that of the base. The skin friction drag coefficient, C_{D_F}, is expressed as

$$C_{D_F} = \frac{C_F S}{q d^2}$$

In this investigation we assumed C_F to be equal to 0.002, a reasonable value at high Reynolds numbers, and thus $C_{D_F} = 0.076$, constant.

Fig. 1 of Ref.10 gives the base pressure coefficient, P_B, defined as

$$P_B = \frac{p_B - p}{q}$$

obtained from various theories and from experiment.

Estimating P_B from these results, we obtained

$$C_{D_B} = \frac{(P - P_B)\left(\frac{\pi}{4} d^2\right)}{q \frac{d^2}{2}} = -\frac{\pi}{q} P_B .$$

C_{D_B} was assumed to be approximately equal to 0.08 for Mach numbers less than 1.0.

The total body drag coefficient, C_{D_1}, is given by

$$C_{D_1} = C_{D_F} + C_{D_N} + C_{D_B}$$

Tail Fin Drag

The proper drag coefficient, C_{D_T}, for the tail fins is defined as

$$C_{D_T} = \frac{1}{2}\left(\frac{D_T}{q S_T}\right)$$

where D_T is the drag of the entire tail (four fins) and S_T is the tail area as previously defined (two fins).

The drag of a thin airfoil at supersonic speed may be considered as being composed of two parts; (1) the pressure or wave drag, and (2) the skin friction. The wave drag may be calculated using Ackeret's small-perturbation theory, and the skin friction estimated from experience with flat plates. Ref. 7 gives the section wave drag coefficient, $C_{D_{TW}}$, for a symmetrical biconvex circular arc airfoil at zero angle of attack as

$$C_{D_{TW}} = \frac{32}{3} \frac{h^2}{\sqrt{M^2 - 1}} , \quad \text{where} \quad h = \frac{1}{2} \frac{t}{c}$$

The skin friction drag coefficient, $C_{D_{TF}}$, was assumed constant and equal to 0.006, a value in good agreement with that predicted and observed for flat plates at large Reynolds numbers.

To obtain the total tail drag coefficient, C_{D_T}, for a given tail configuration, it is only necessary to apply the relation

$$C_{D_T} = \frac{D_T}{q d^2} = C_{D_\pi} \times 2 \frac{S_T}{d^2}$$

The values of C_{D_π} as a function of Mach number appear in Fig. (10).

Values of the total drag coefficient for the complete rocket, $C_D = C_{D_1} + C_{D_T}$, are presented in Fig. (11). This figure also shows a comparison of the calculated drag coefficient with that obtained experimentally by the Germans for the A-4 missile (Ref. 12). The comparison indicates good qualitative agreement.

IV. EQUATION OF MOTION AND THE EFFECT OF ROCKET PARAMETERS ON THE TRAJECTORY IN VACUUM

The general equation of motion for a rocket in vertical flight is

$$F - D - W = \frac{W}{g}\frac{dv}{dt} \qquad [4.1]$$

If we assume that during powered flight the thrust and the rate of fuel consumption of the rocket motor are constant, the weight, W, at any instant of time, t, can be expressed as

$$W = W_0\left(1 - \nu\frac{t}{t_p}\right) \qquad [4.2]$$

where W_0 is the initial gross weight, ν is the propellant weight ratio $\frac{W_F}{W_0}$, and t_p is the time at which the propellant will have been exhausted.

The thrust, F, is given by

$$F = I\,\frac{W_F}{t_p} \qquad [4.3]$$

where $\frac{W_F}{t_p}$ is the rate of propellant consumption and I is the specific impulse, which is a property of the propellant.

The drag, D, has been defined as

$$D = \tfrac{1}{2}\rho V^2 C_D d^2 .$$

The variation of the density, ρ, with altitude in the standard atmosphere is given by the relation $\rho = \rho_0\,\sigma$, where σ, the density ratio, is a function of the altitude only.

It is found convenient in the study of rockets of various shapes to introduce the loading factor, $\mu = \frac{W_0}{d^2}$. In the discussion of Section V, we chose a single value of μ which gave an initial gross weight compatible with the dimensions of our

rocket, and did not investigate the effects of varying μ.

In terms of I, ν, and t_p, the equation of motion for powered flight becomes

$$\frac{dv}{dt} = \left(\frac{\frac{I\nu}{t_p} - \frac{1}{2}\rho_0 \sigma C_D v^2 \frac{1}{\mu}}{1 - \nu \frac{t}{t_p}} - 1 \right) g \qquad [4.4]$$

In coasting flight, after the propellant is consumed, the thrust is zero and the weight is constant, $W = W_0 (1-\nu)$.

The equation of motion for the unpowered condition becomes

$$\frac{dv}{dt} = -\left(\frac{\frac{1}{2}\rho_0 \sigma C_D v^2 \frac{1}{\mu}}{1-\nu} + 1 \right) g \qquad [4.5]$$

In the sounding rocket performance analysis, we are most interested in determining the maximum altitude, y_s, that the rocket can reach. To obtain this it is necessary to integrate the Eqs. [4.4] and [4.5], using the initial conditions $y = 0$, $v = v_0$ at $t = 0$. ($v_0 = 0$ for all cases considered here). These equations are not directly integrable in the general case, but various approximate methods of evaluation are available (Refs. 13 and 14). In Section V the method of stepwise numerical integration was employed.

In the special case where the drag term is neglected and the acceleration of gravity, g, is considered constant, Eq. [4.4] becomes

$$\frac{dv}{dt} = g\left(\frac{\frac{I\nu}{t_p}}{1 - \nu \frac{t}{t_p}} - 1 \right) \qquad 0 \le t \le t_p \qquad [4.6]$$

and can be directly integrated to give

$$v = -gI \ln \left(1 - \frac{\nu}{t_p} t\right) - gt + v_0$$

Thus,

$$y = \frac{I}{\nu} g t_p \left(1 - \frac{\nu}{t_p} t\right) \ln \left(1 - \frac{\nu}{t_p} t\right) + Igt - \frac{1}{2} g t^2 + v_0 t$$

At the end of burning, $t = t_p$,

$$V_p = -gI\ln(1-\nu) - gt_p \qquad [4.7]$$

and

$$y_p = \frac{I}{\nu}g t_p (1-\nu)\ln(1-\nu) + Igt_p - \frac{1}{2}gt_p^2 \qquad [4.8]$$

The additional altitude, y_c, gained in coasting flight <u>in vacuo</u>, may be obtained by equating the kinetic energy at end of burning to the increase in potential energy in coasting to zero velocity:

$$y_c = \frac{V_p^2}{2g} \qquad [4.9]$$

The summit altitude is then

$$y_s = y_p + y_c = \frac{1}{2g}[V_0 - gI\ln(1-\nu)]^2 + \frac{I}{\nu}g t_p [\nu + \ln(1-\nu)] \qquad [4.10]$$

Using Eqs. [4.7], [4.8], and [4.10], we calculated V_p, y_p, and y_s for various I, ν, and t_p. The values chosen for this study were:

$$I = 150, 200, 300, 400 \ \frac{\text{LB SEC}}{\text{LB}}$$
$$\nu = 0.5, 0.7, 0.9$$
$$t_p = 15, 30, 45, 60 \ \text{SEC}$$

The results of these calculations are plotted in Figs. (12) through (23). It is seen that the greatest summit altitude is attained when the burning time is zero; i. e., when the rocket is shot as a free projectile from $y = 0$. This is of course not the case in the actual air trajectory, since the attainment of high velocities early in flight results in tremendous losses due to drag in the dense lower air, and reduces the maximum altitude reached. It will be observed in Section V that there is in general an optimum t_p for each combination of I and ν which gives the maximum summit altitude.

A word may be said about the values of I and η investigated: good present-day fuels give specific impulses of the order of 200 lb sec/lb; η of 0.7 is a fairly high value compared with present practice. Thus, it can be seen that the investigation extends into a range of values whose attainment is not probable in the immediate future. Further conclusions on this subject are drawn in Section V after examination of the air trajectories. One criterion for determining the range of values of I, η and t_p that may be used in design is the initial acceleration at take-off, $\frac{F}{W_0}$. The acceleration should in general be greater than 2g, but excessively high values are to be avoided for structural reasons. Values of the initial acceleration as a function of burning time for various I and η are presented in Figs. (24) through (27), as calculated from the relation

$$\frac{F}{W_0} = \frac{I\eta}{t_p} \qquad [4.11]$$

An additional and most important consideration is as follows: the assumption of constant gravitational acceleration, under which these trajectories were calculated, is definitely invalid when y_s is of the order of 1000 miles. It is known that the acceleration of gravity follows the inverse square law

$$g = g_0 \left(\frac{R}{R+y}\right)^2 \qquad [4.12]$$

where g_0 is the acceleration of gravity at the surface of the Earth, R is the radius of the Earth, and y is the altitude above the surface. Fig. (28) is a plot of Eq. [4.12] for altitudes of interest in this investigation.

Tsien and Malina (Ref. 2) deduce the following correction function for the actual altitude gained during coasting as compared with that calculated assuming constant g:

$$y_{cg} = y_c\left[1 + \left(\frac{y_c}{y_p + R}\right) + \left(\frac{y_c}{y_p + R}\right)^2 + \cdots\right] \qquad [4.13]$$

in which

y_{cg} is the actual altitude gained,

y_c is as calculated using g constant and equal to g at altitude y_p,

and R is the radius of the Earth.

Application of this formula to one extreme case, $I = 400$, $v = 0.9$, and $t_p = 60$ sec, for which $y_p \doteq 98$ mi. and $y_c \doteq 2300$ mi., gave a corrected summit altitude, y_{sg}, of about 5200 miles, more than twice the previously calculated value. In the air trajectory calculations of Section V no such extreme influence of the variation in g is observed, because the altitudes reached are much lower. The effect is, however, of significant magnitude in several cases.

V. PERFORMANCE OF SOUNDING ROCKET IN THE STANDARD ATMOSPHERE

Approximate solutions of the equations of motion for rocket flight in air may be obtained by various methods, some of which are discussed in Refs. 13 and 14. The method of stepwise numerical integration, which was used in the present analysis, is relatively simple and rapid and gives reasonably accurate results.

The results of the calculations for nine trajectories, based on the NACA standard atmosphere as given in Refs. 7 and 15, are presented in Table I. The cases calculated were one each for four values of burning time in two configurations of the rocket, and a comparison trajectory to illustrate the effect of errors in the estimation of drag. The two configurations chosen were:

(1) Design Mach number = 8, $\mu = 2000$, $\nu = 0.7$, $W_o = 18{,}000$ LB, $I = 200$ LB SEC/LB, $t_p = 15, 30, 45$ AND 60 SEC.

(2) Design Mach number = 10, $\mu = 2000$, $\nu = 0.7$, $W_o = 18{,}000$ LB, $I = 400$ LB SEC/LB, $t_p = 15, 30, 45$ AND 60 SEC.

The comparison trajectory was calculated for Configuration (2), $t_p = 60$ SEC, but the drag coefficient corresponding to a design Mach number of 8 was used. The comparison of the corrected summit altitudes, y_{s_g}, shows only about 4% difference in y_{s_g} for a 15% difference in the drag coefficients.

It may be seen from Table I that in all cases for $I = 400$ the design Mach number is exceeded. Therefore longitudinal instability will occur, unless larger fins or auxiliary means of achieving stability are used. It is also noted that the maximum acceleration,

which occurs at the instant before burnout, is in several cases of such magnitude as to create severe structural or instrumentation problems.

In Figs. (29), (30), and (31) is presented a comparison of velocity at end of burning, V_{P_g}, altitude at end of burning, y_{P_g}, and summit altitude, y_{S_g}, as calculated by numerical integration, with the corresponding quantities V_P, y_P, and y_S as determined in Section IV under the assumptions of constant gravity and no drag. It will be noted from Fig. (31) that in the region of burning time corresponding to optimum performance, i. e., y_{S_g} maximum, there is little difference between the summit altitudes as calculated by the two methods. The conclusion is that the error due to neglecting variation in gravity tends to cancel the error due to neglecting drag. Thus, vacuum trajectory calculations made under the assumption of constant gravity may have more value than has hitherto been supposed.

VI. CONCLUSIONS

The conclusions reached in the sounding rocket performance analysis presented in this Thesis are as follows:

1. It is apparently practical to fin-stabilize a rocket designed to reach a flight Mach number of 10, but at higher Mach numbers the fins required become excessively large.

2. Errors in the estimation of drag coefficient do not greatly influence the ultimate performance.

3. If the specific impulse of the propellant can be increased from 200 to 400 lb sec/lb, the summit altitude will be of the order of six times its previous value.

4. For the configurations of the rocket which were investigated, there is apparently an optimum burning time of approximately 35 sec., but its use may be limited in the case of high specific impulse by the acceleration or by the Mach number attained. In the case where $I = 400$, there is a fairly wide range of burning times which may be used without much loss of performance.

5. The vacuum trajectory calculated assuming constant gravity gives in this case a close approximation to the actual trajectory corrected for air resistance and the variation of g with altitude; further investigation to determine the generality of this correspondence is warranted.

REFERENCES

1. F.J. Malina and A.M.O. Smith: "Flight Analysis of the Sounding Rocket", J. Ae. Sci., Vol. 5, No. 5, 1938

2. H.S. Tsien and F.J. Malina: "Flight Analysis of the Sounding Rocket with Special Reference to Propulsion by Successive Impulses", J. Ae. Sci., Vol. 6, No. 2, 1938

3. H.S. Siefert, M.M.Mills, and M. Summerfield: "The Physics of Rockets: Dynamics of Long Range Rockets", Am. J. Phys., Vol. 15, No. 3, 1947

4. H.S. Tsien: "Supersonic Flow over an Inclined Body of Revolution", J. Ae. Sci., Vol. 5, No. 12, 1938

5. E.V. Laitone: "The linearized Subsonic and Supersonic Flow About Inclined Slender Bodies of Revolution", J. Ae. Sci., Vol. 14, No. 11, 1947

6. F. Wienig: "Lift and Drag of Wings with Small Span", NACA TM 1151, 1947

7. "Notes and Tables for use in the Analysis of Supersonic Flow", NACA TN 1428, 1947

8. T.H. von Karman and N.B. Moore: "Resistance of slender Bodies Moving with Supersonic Velocities, with Special Reference to Projectiles", Trans. A.S.M.E., 1932

9. A.C. Charters and R.A. Turetsky: "Determination of Base Pressure from Free Flight Data", B. R. L. Report 653, 1948

10. Dean Chapman: "Base Pressure at Supersonic Velocities", Thesis, 1948, California Institute of Technology

References (Cont.)

11. Z. Kopal: "Supersonic Flow around Cones", M.I.T., 1947

12. Kochel Report 66/33, Peenemunde, 1944

13. T.H. von Karman and M.A. Biot:"Mathematical Methods in Engineering", McGraw-Hill, 1940

14. G.A. Bliss: "Mathematics for Exterior Ballistics", Wiley, 1944

15. C.N. Warfield: "Tentative Tables for the Properties of the Upper Atmosphere", NACA TN 1200, 1947

TABLE I

RESULTS OF NUMERICAL INTEGRATION

Configuration (1) : $I = 200$, Design Mach No. = 8

t_p	v_{p_g}	y_{p_g}	y_{s_g}	a_{max}	M_{max}
15 sec.	6394 $\frac{ft.}{sec.}$	39,960 ft.	530,000 ft.	21.25 g	6.59
30	5894	70,580	590,000	12.93	6.07
45	5559	95,909	580,000	8.82	5.73
60	5196	114,792	543,000	6.99	5.10

Configuration (2) : $I = 400$, Design Mach No. = 10

t_p	v_{p_g}	y_{p_g}	y_{s_g}	a_{max}	M_{max}
15	13,313	81,854	3,056,000	49.77	11.33
30	13,305	155,425	3,368,000	27.75	12.73
45	13,090	224,802	3,335,000	18.35	11.50
60	12,763	288,000	3,203,000	14.18	12.50

Comparison Trajectory: $I = 400$, Design Mach No. = 8

t_p	v_{p_g}	y_{p_g}	y_{s_g}	a_{max}	M_{max}
60	12,868	291,235	3,329,000	14.18	12.65

INDEX OF FIGURES

CONFIGURATION SHOWN:

$C_0 = 10.78$ FT ~ $M_{DES} = 8$

$\frac{\ell}{d} = 14.0$

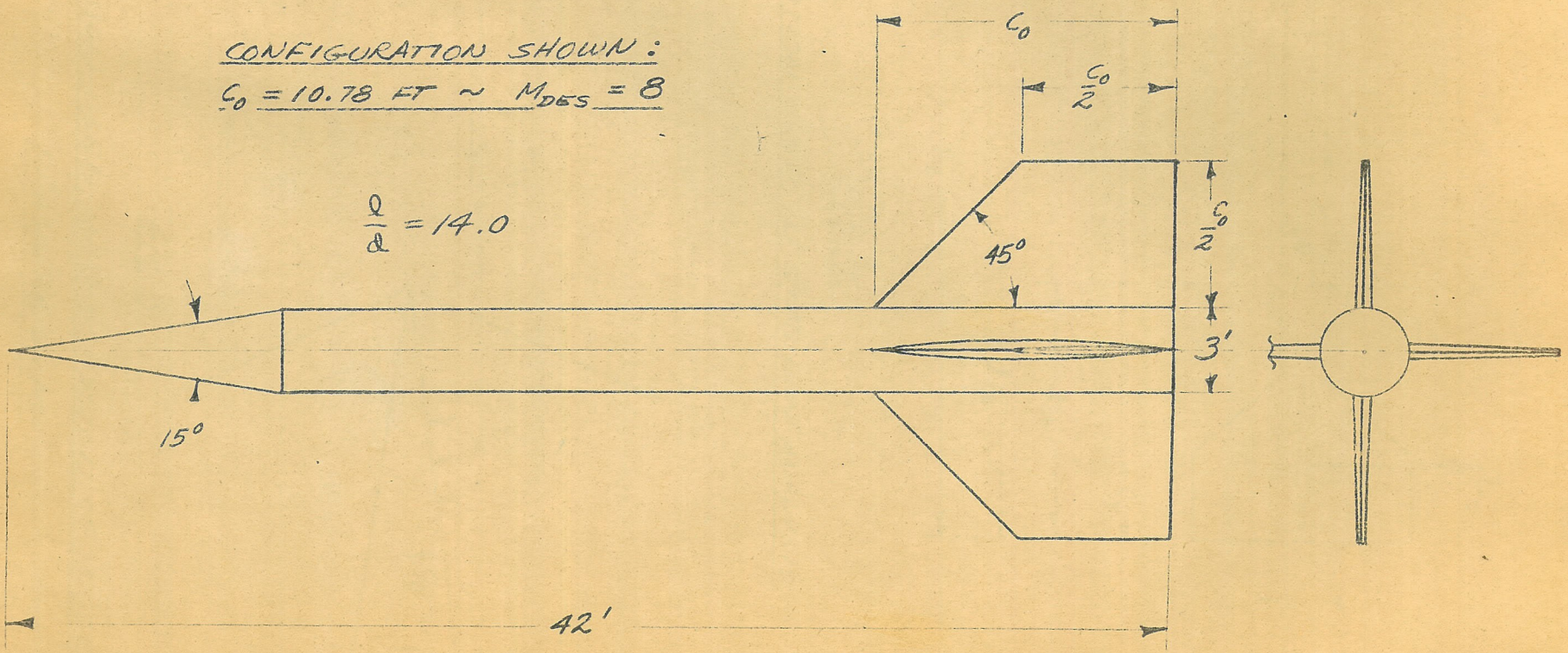

FIG: 1

BASIC DIMENSIONS OF ROCKET

SCALE: 1" = 6'

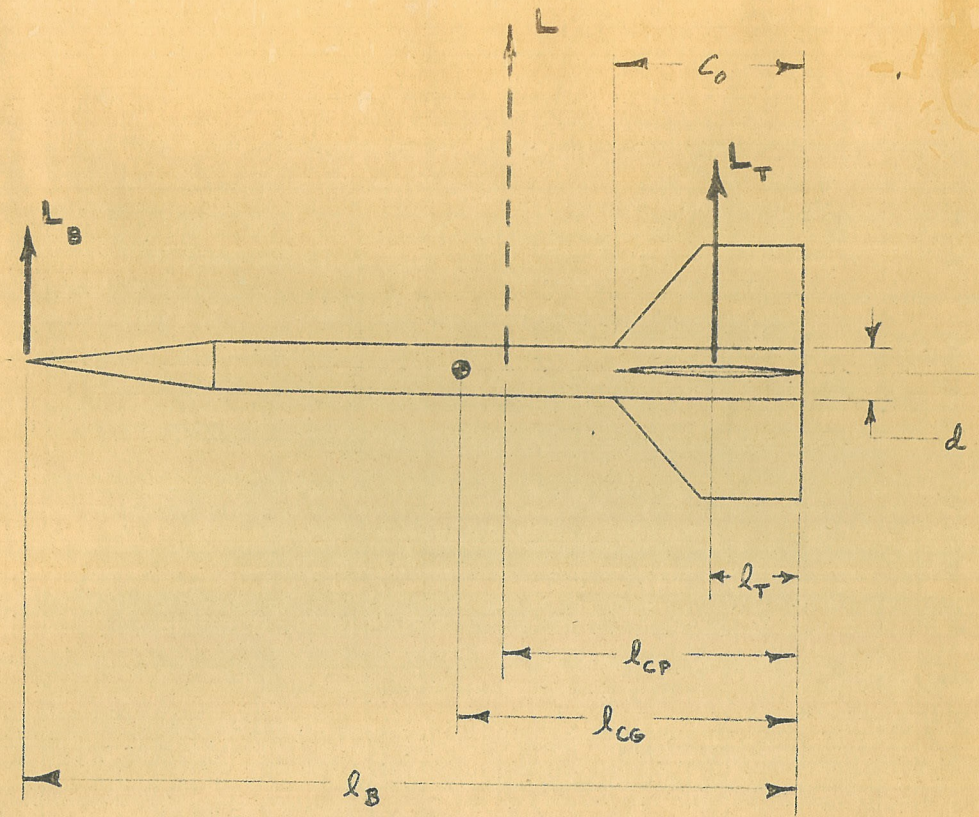

FIG. 2.

NOTATION USED IN STABILITY ANALYSIS

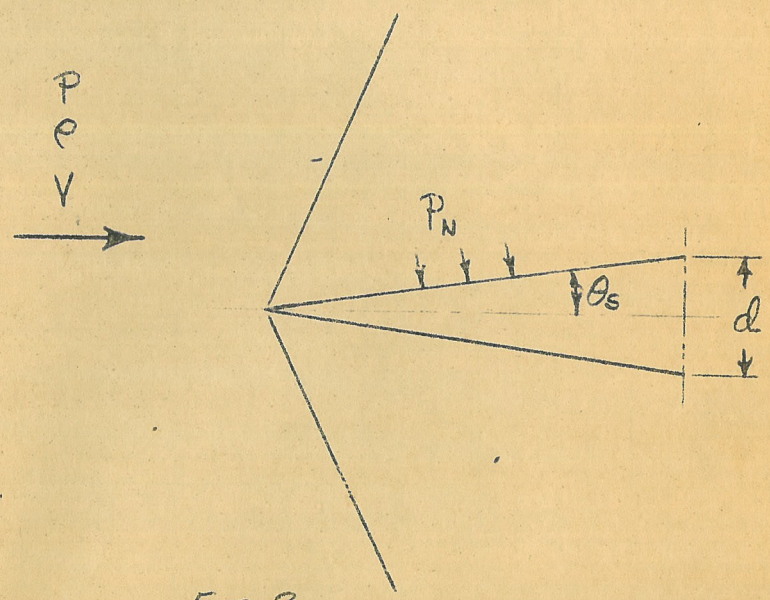

FIG. 3

NOTATION USED IN DISCUSSION OF NOSE PRESSURE DRAG

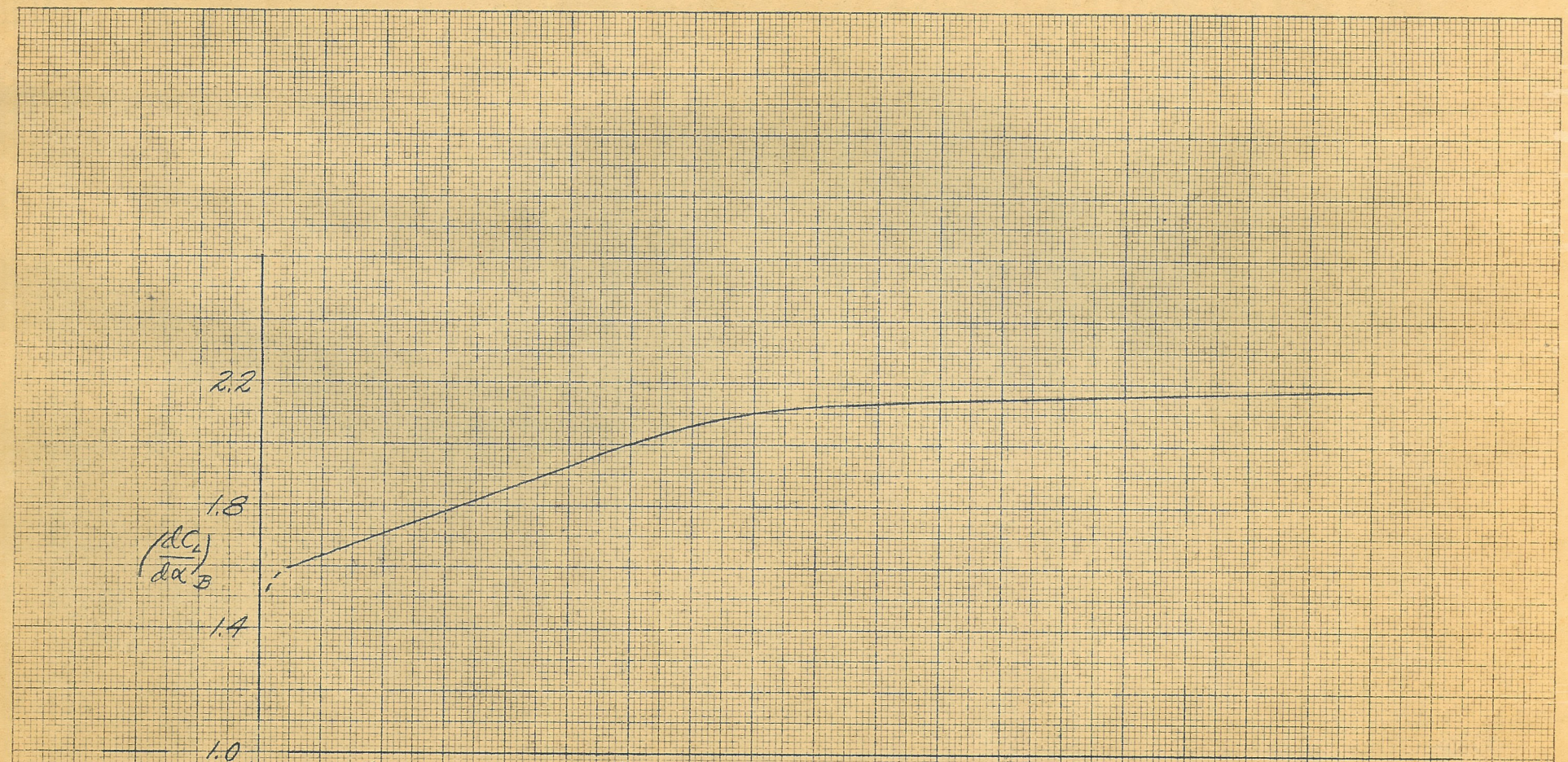

$\left(\frac{dC_L}{d\alpha}\right)_B$ VS MACH NO. FOR BODY

$C_{L_B} = \frac{L_B}{\frac{1}{2}\rho V^2}$

PAGE 29
FIG. 4

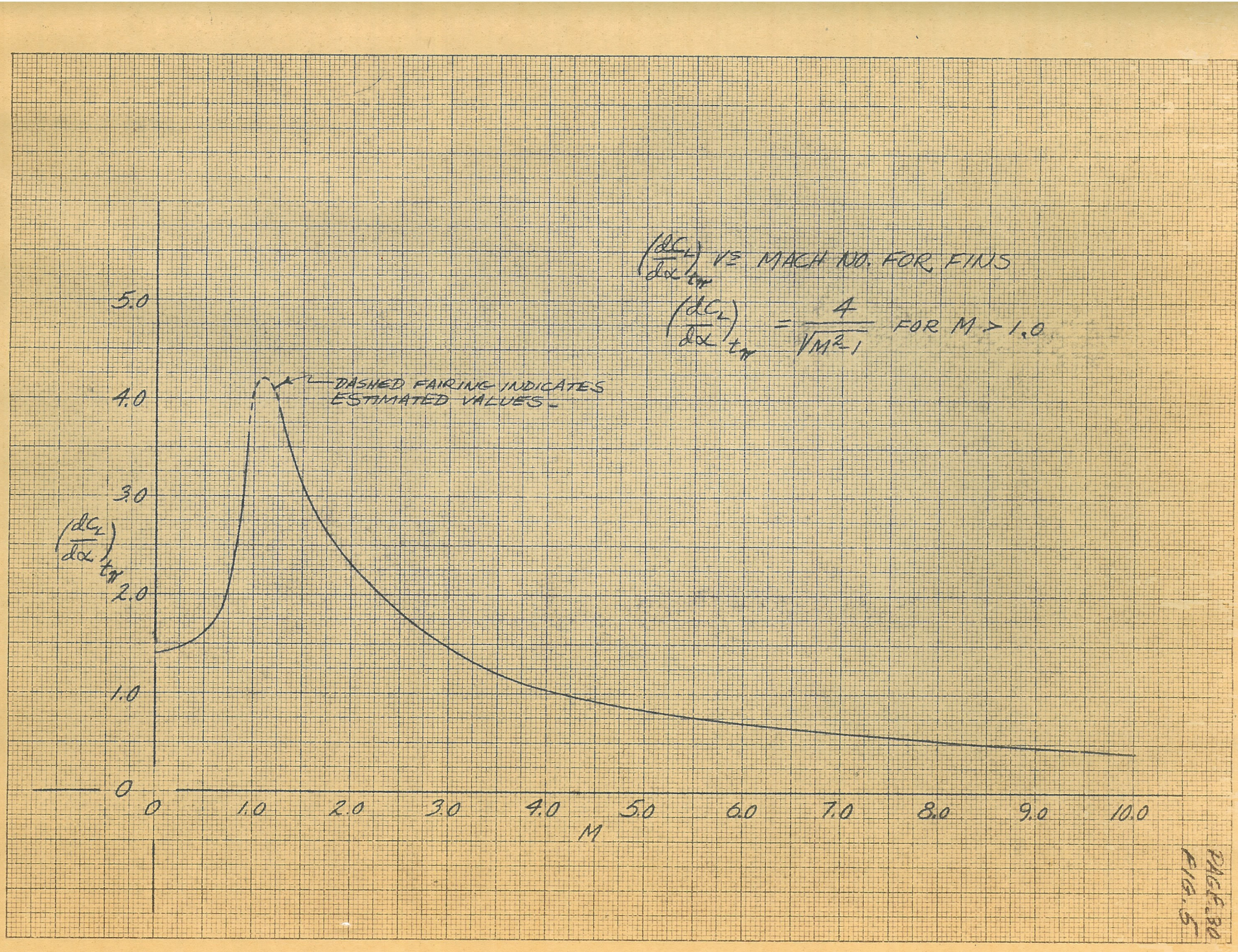
$\left(\frac{dC_L}{d\alpha}\right)_{t_N}$ VS MACH NO. FOR FINS
$\left(\frac{dC_L}{d\alpha}\right)_{t_N} = \frac{4}{\sqrt{M^2-1}}$ FOR $M > 1.0$
DASHED FAIRING INDICATES ESTIMATED VALUES
$\left(\frac{dC_L}{d\alpha}\right)_{t_N}$
5.0
4.0
3.0
2.0
1.0
0
0
1.0
2.0
3.0
4.0
5.0
6.0
7.0
8.0
9.0
10.0
M
PAGE 30
FIG. 5

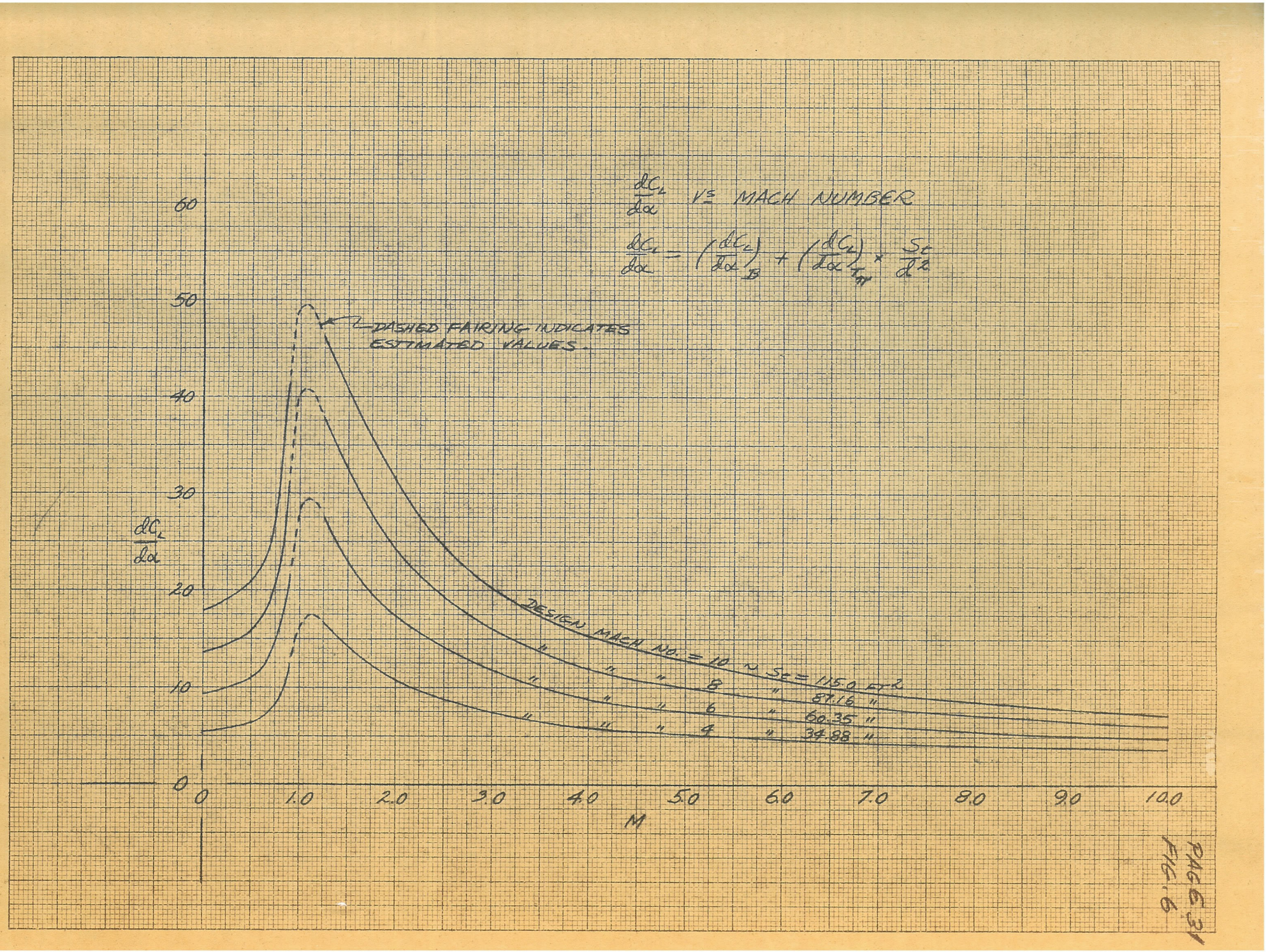
$\frac{dC_L}{d\alpha}$ VS MACH NUMBER
$\frac{dC_L}{d\alpha} = \left(\frac{dC_L}{d\alpha}\right)_B + \left(\frac{dC_L}{d\alpha}\right)_{T_H} \times \frac{S_c}{d^2}$
DASHED FAIRING INDICATES ESTIMATED VALUES.
DESIGN MACH NO. = 10 ~ S_c = 115.0 FT²
" " " 8 " 87.16 "
" " " 6 " 60.35 "
" " " 4 " 34.88 "
$\frac{dC_L}{d\alpha}$
M
0
10
20
30
40
50
60
1.0
2.0
3.0
4.0
5.0
6.0
7.0
8.0
9.0
10.0

PAGE 31
FIG. 6

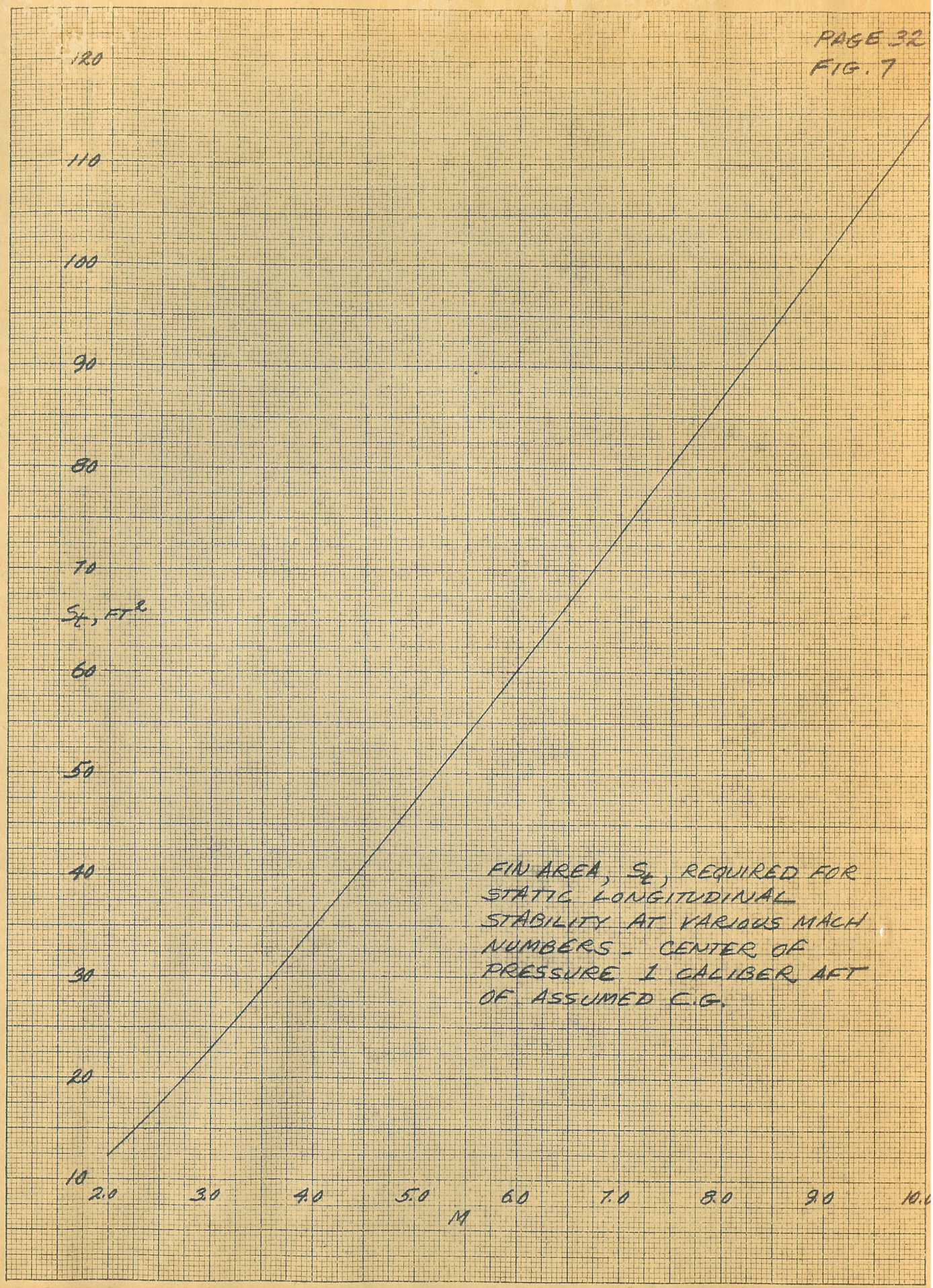

FIN AREA, S_t, REQUIRED FOR STATIC LONGITUDINAL STABILITY AT VARIOUS MACH NUMBERS - CENTER OF PRESSURE 1 CALIBER AFT OF ASSUMED C.G.

CENTER OF PRESSURE LOCATION VS MACH NUMBER FOR VARIOUS TAIL AREAS, $S_t = 0.75 c_o^2$

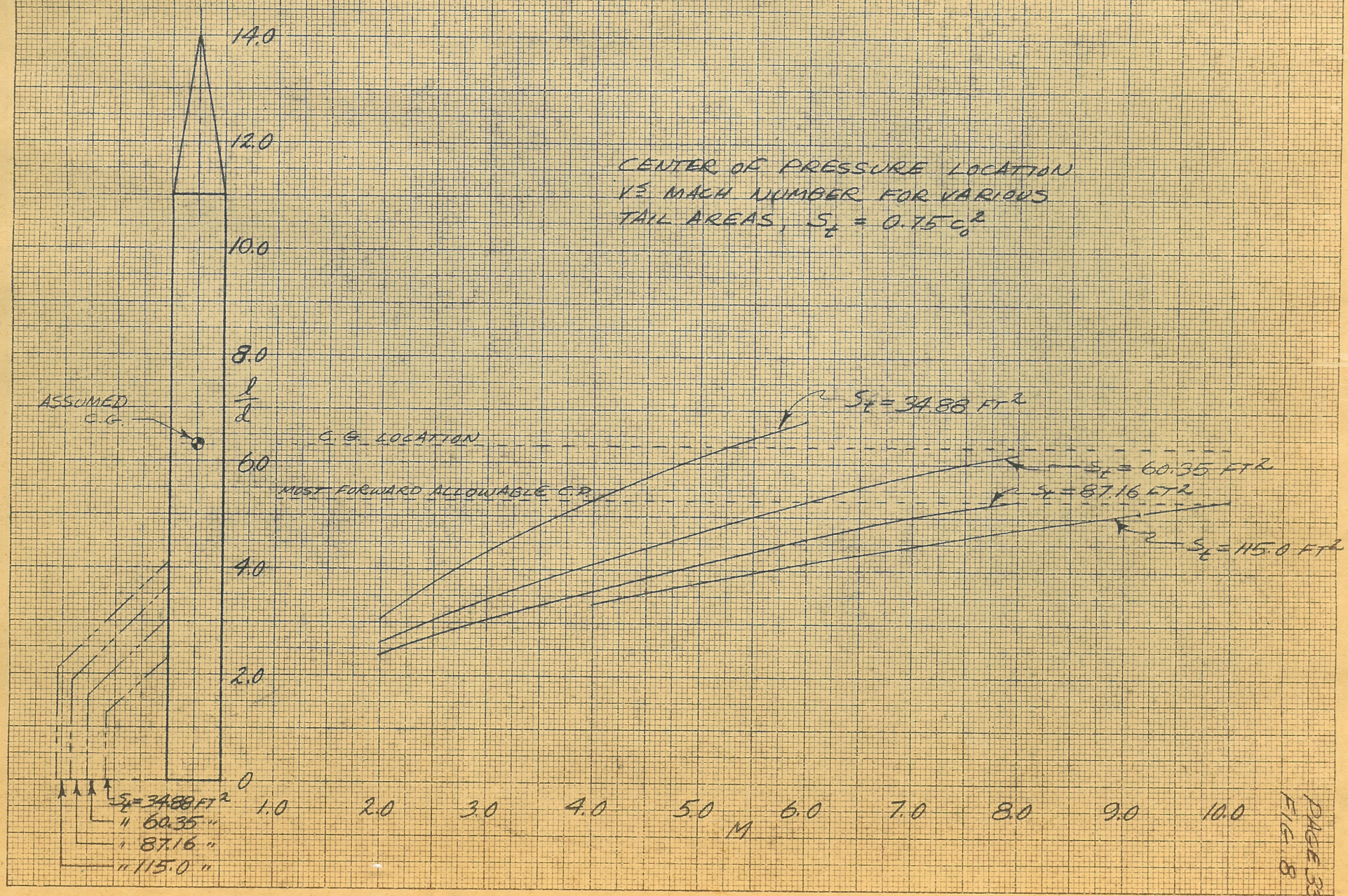

FIG. 8

PAGE 33

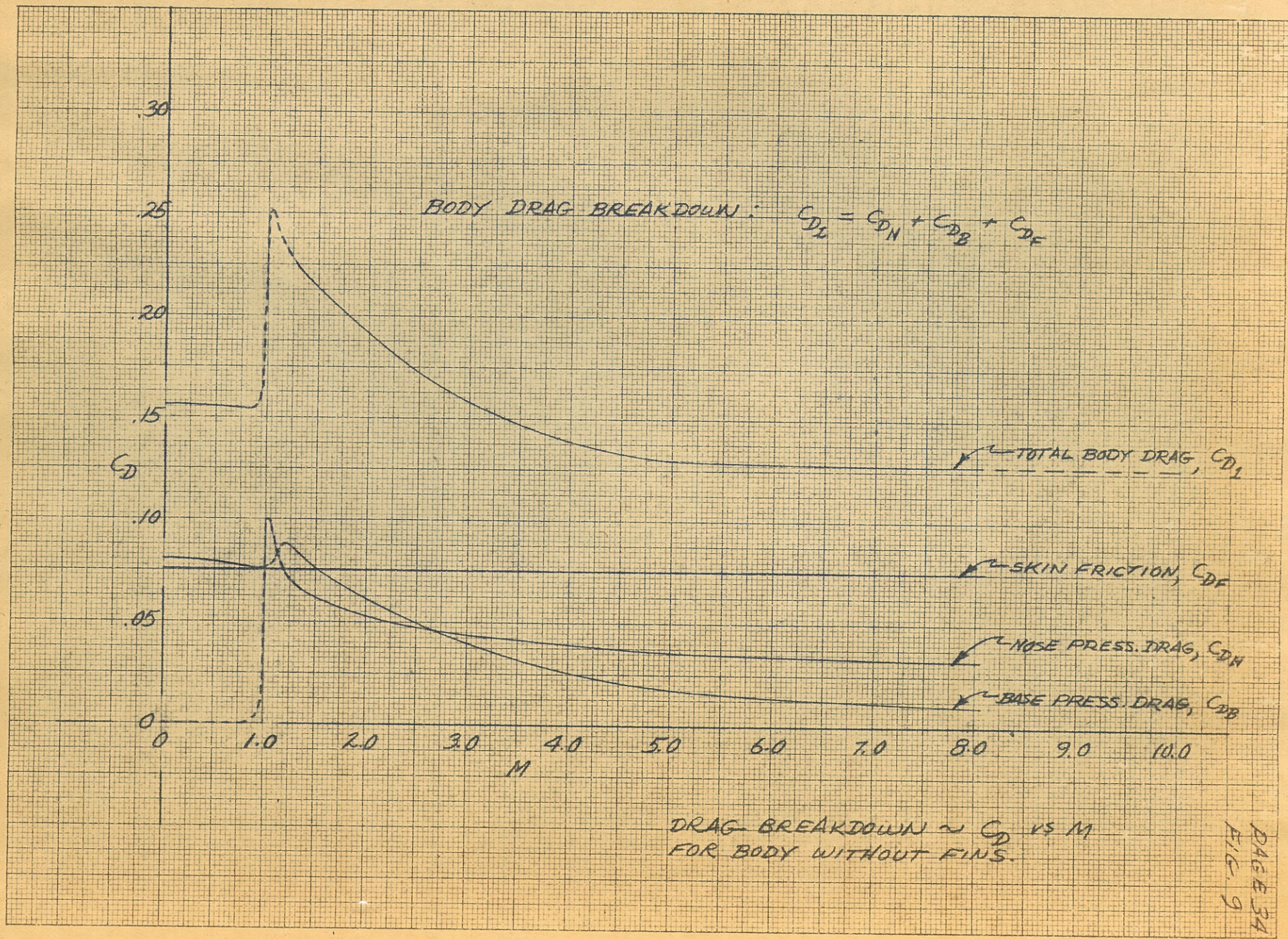

DRAG BREAKDOWN ~ C_D vs M
FOR BODY WITHOUT FINS.

PAGE 34
FIG. 9

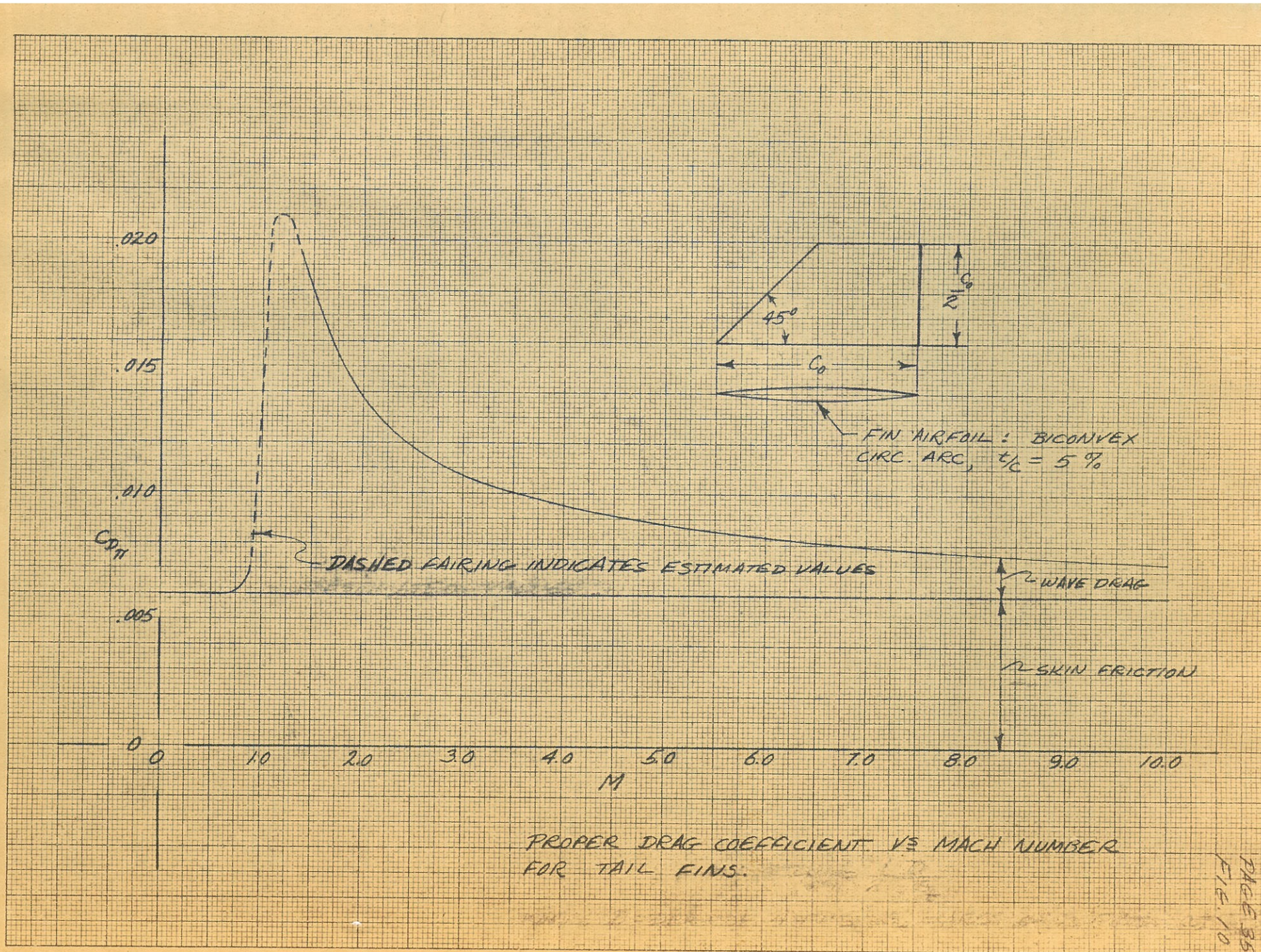

PROPER DRAG COEFFICIENT VS MACH NUMBER FOR TAIL FINS.

PAGE 85
FIG. 10

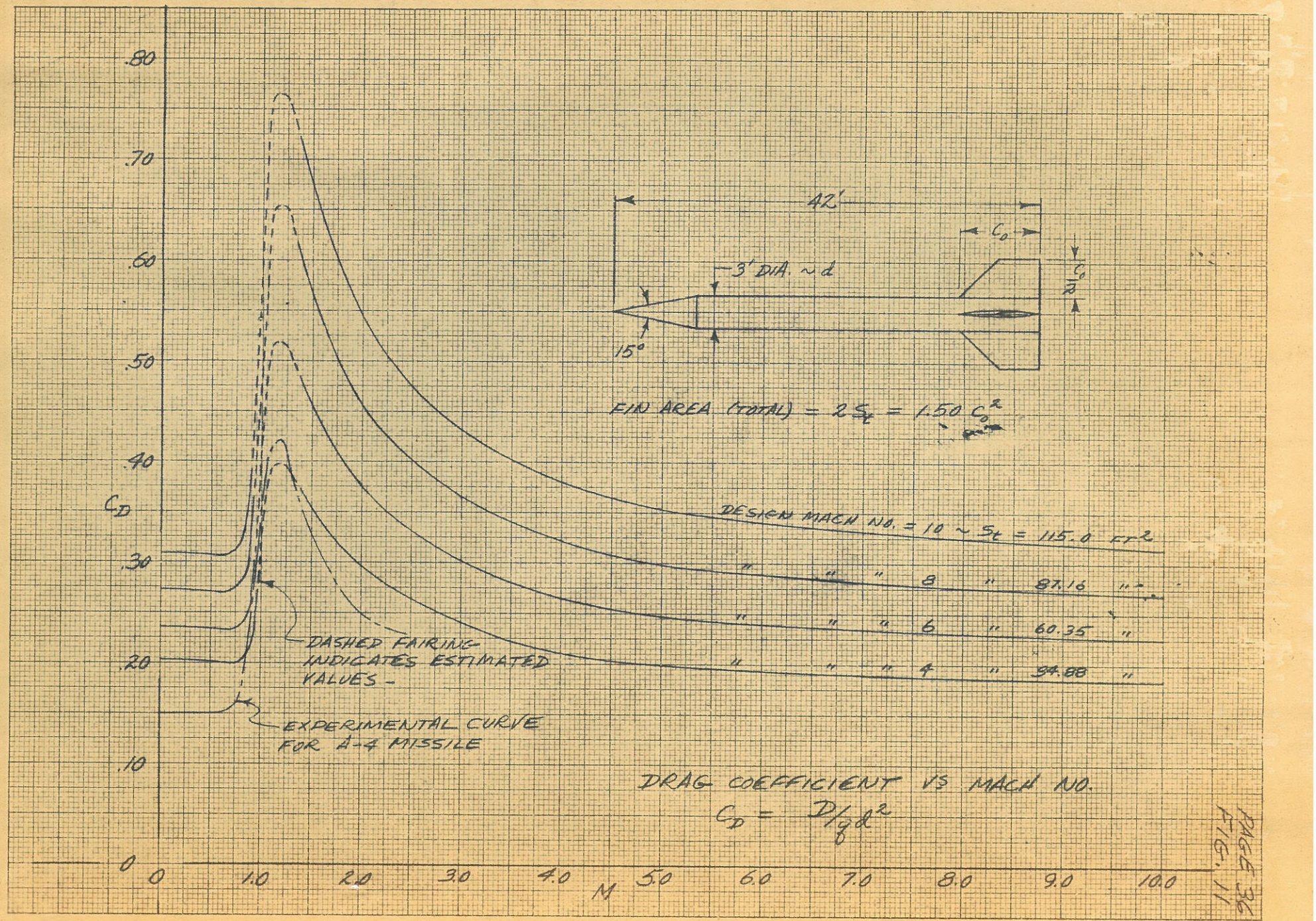

DRAG COEFFICIENT VS MACH NO.

$C_D = D/qd^2$

PAGE 36
FIG. 11

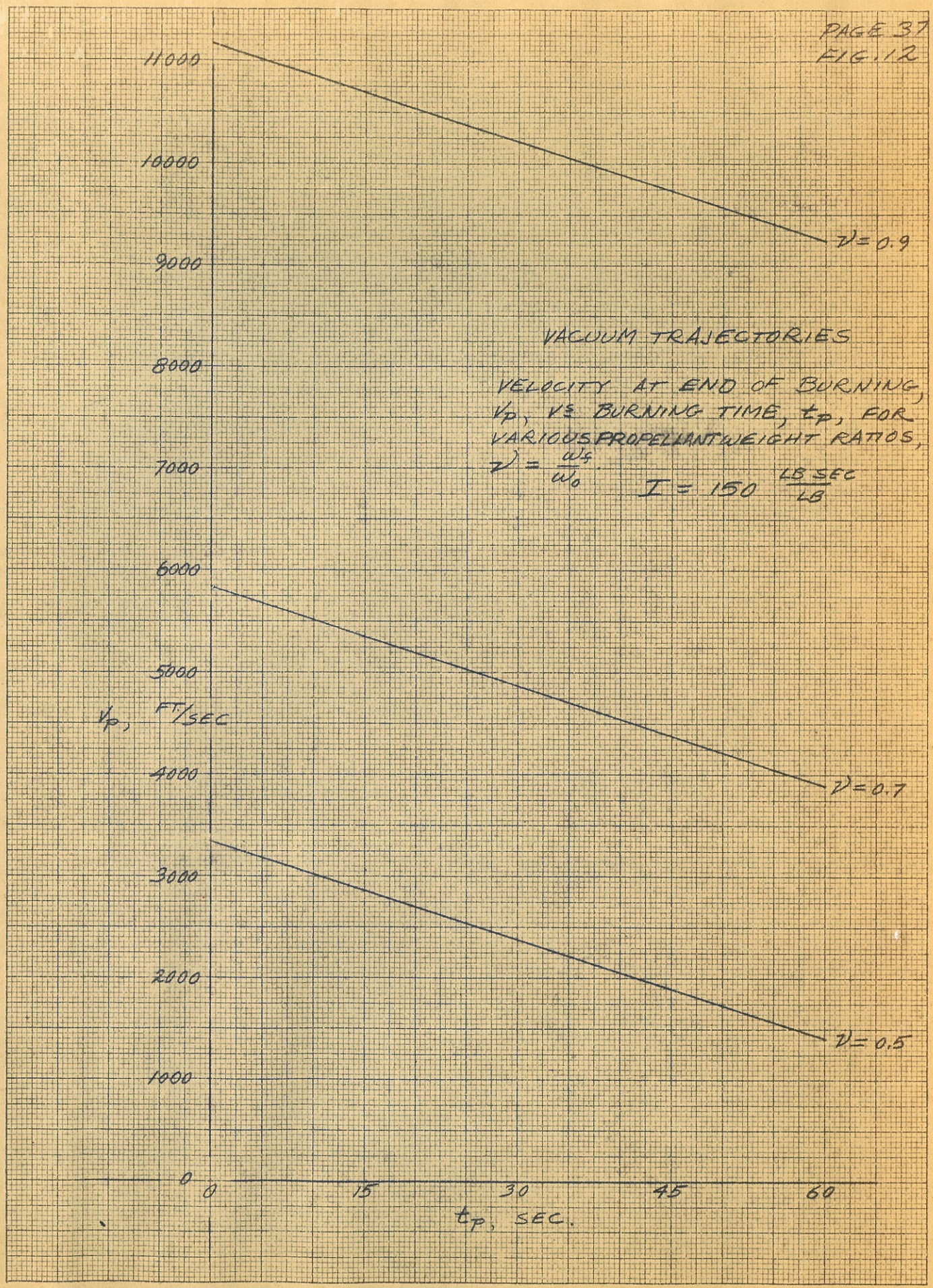
11000
10000
9000
8000
7000
6000
5000
4000
3000
2000
1000
0
V_p, FT/SEC
0
15
30
45
60
t_p, SEC.
$\nu = 0.9$
$\nu = 0.7$
$\nu = 0.5$
VACUUM TRAJECTORIES
VELOCITY AT END OF BURNING, V_p, VS. BURNING TIME, t_p, FOR VARIOUS PROPELLANT WEIGHT RATIOS, $\nu = \frac{w_s}{w_0}$.
$I = 150 \frac{LB\ SEC}{LB}$

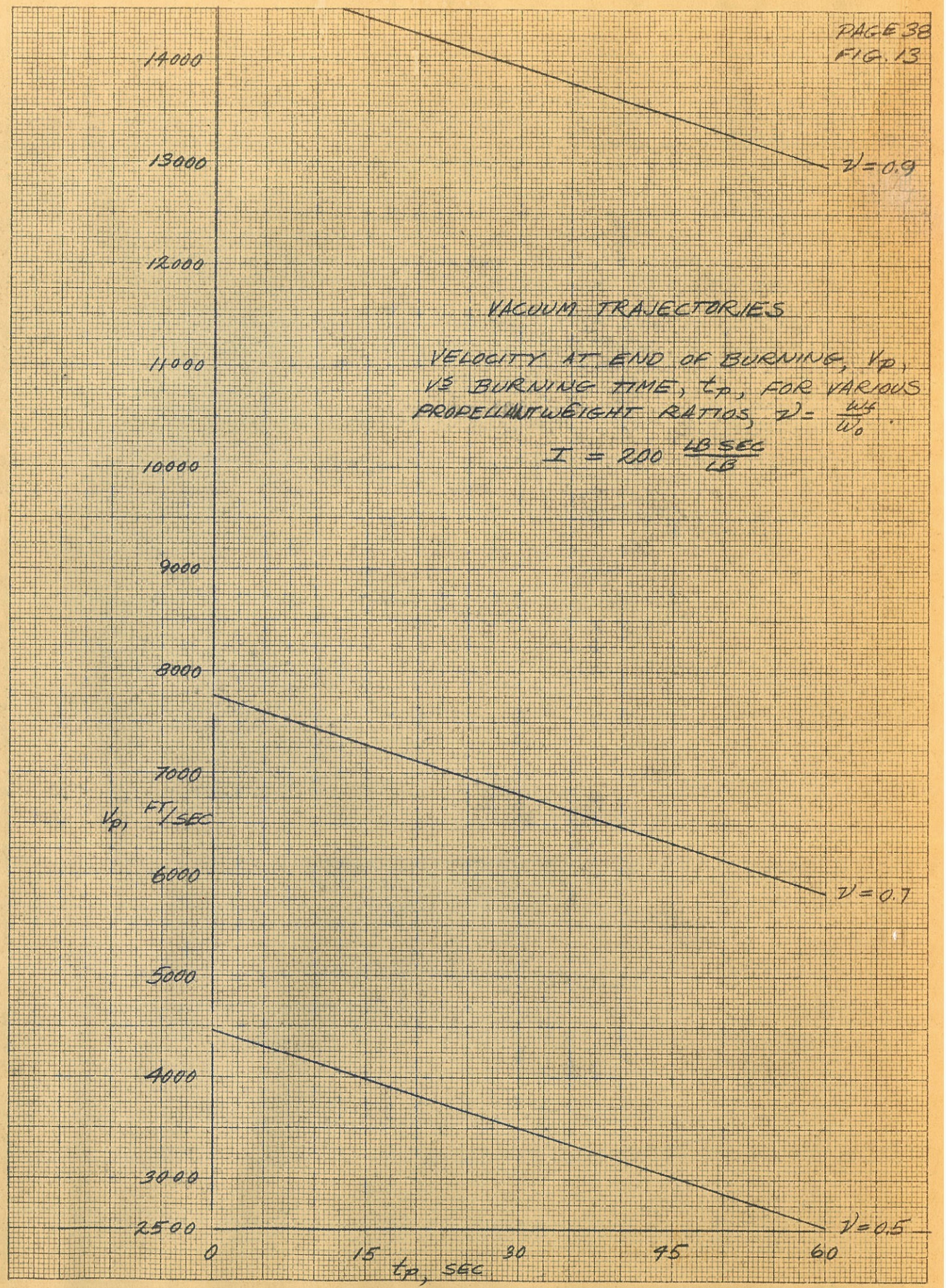
VACUUM TRAJECTORIES
VELOCITY AT END OF BURNING, V_p, VS BURNING TIME, t_p, FOR VARIOUS PROPELLANT WEIGHT RATIOS, $\nu = \frac{w_f}{w_o}$.
$I = 200 \frac{LB\ SEC}{LB}$
14000
13000
12000
11000
10000
9000
8000
7000
6000
5000
4000
3000
2500
V_p, FT/SEC
0
15
30
45
60
t_p, SEC
$\nu = 0.9$
$\nu = 0.7$
$\nu = 0.5$

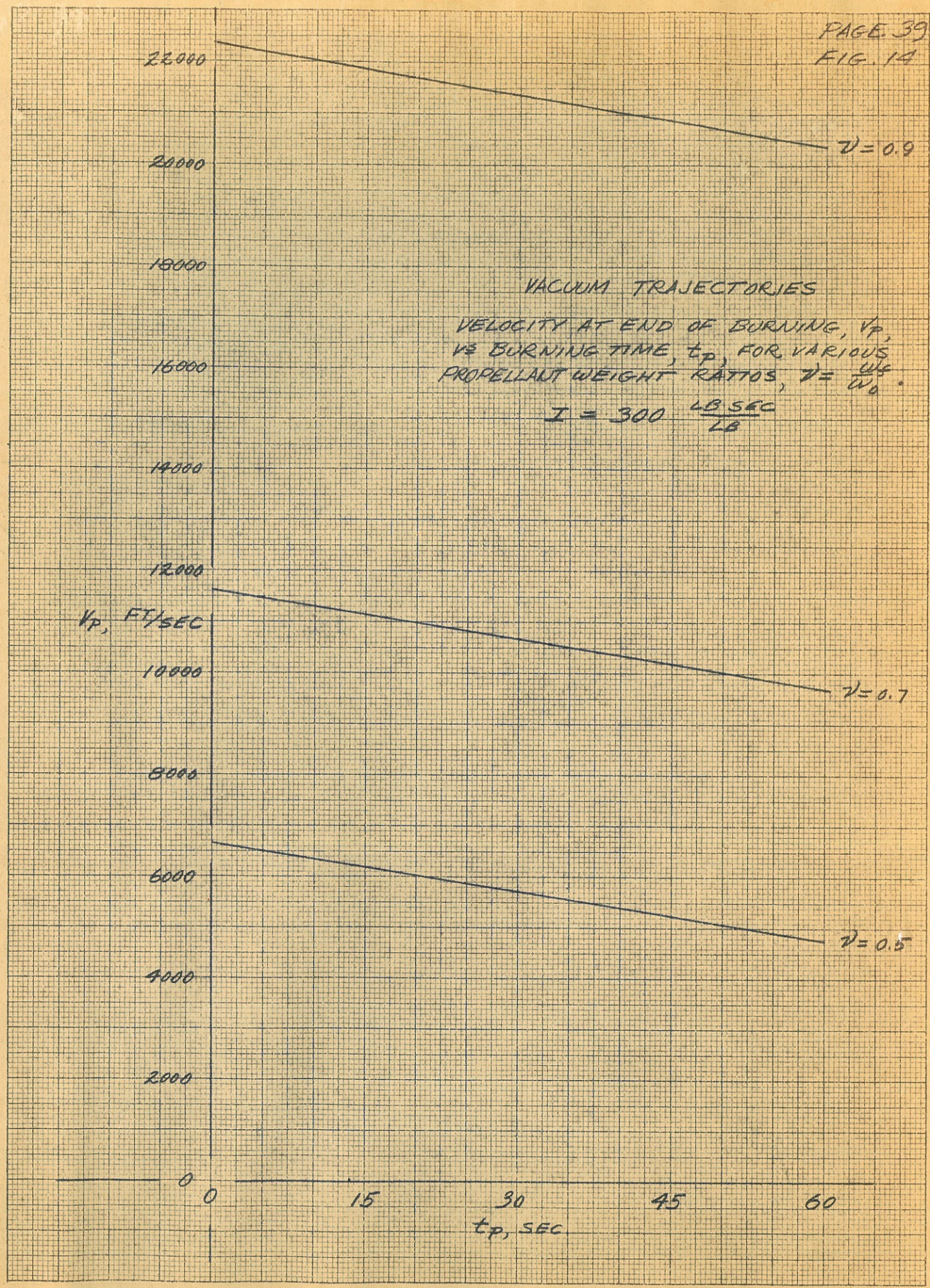

VACUUM TRAJECTORIES

VELOCITY AT END OF BURNING, V_p, VS BURNING TIME, t_p, FOR VARIOUS PROPELLANT WEIGHT RATIOS, $\nu = \frac{W_f}{W_0}$.

$I = 300 \frac{LB\,SEC}{LB}$

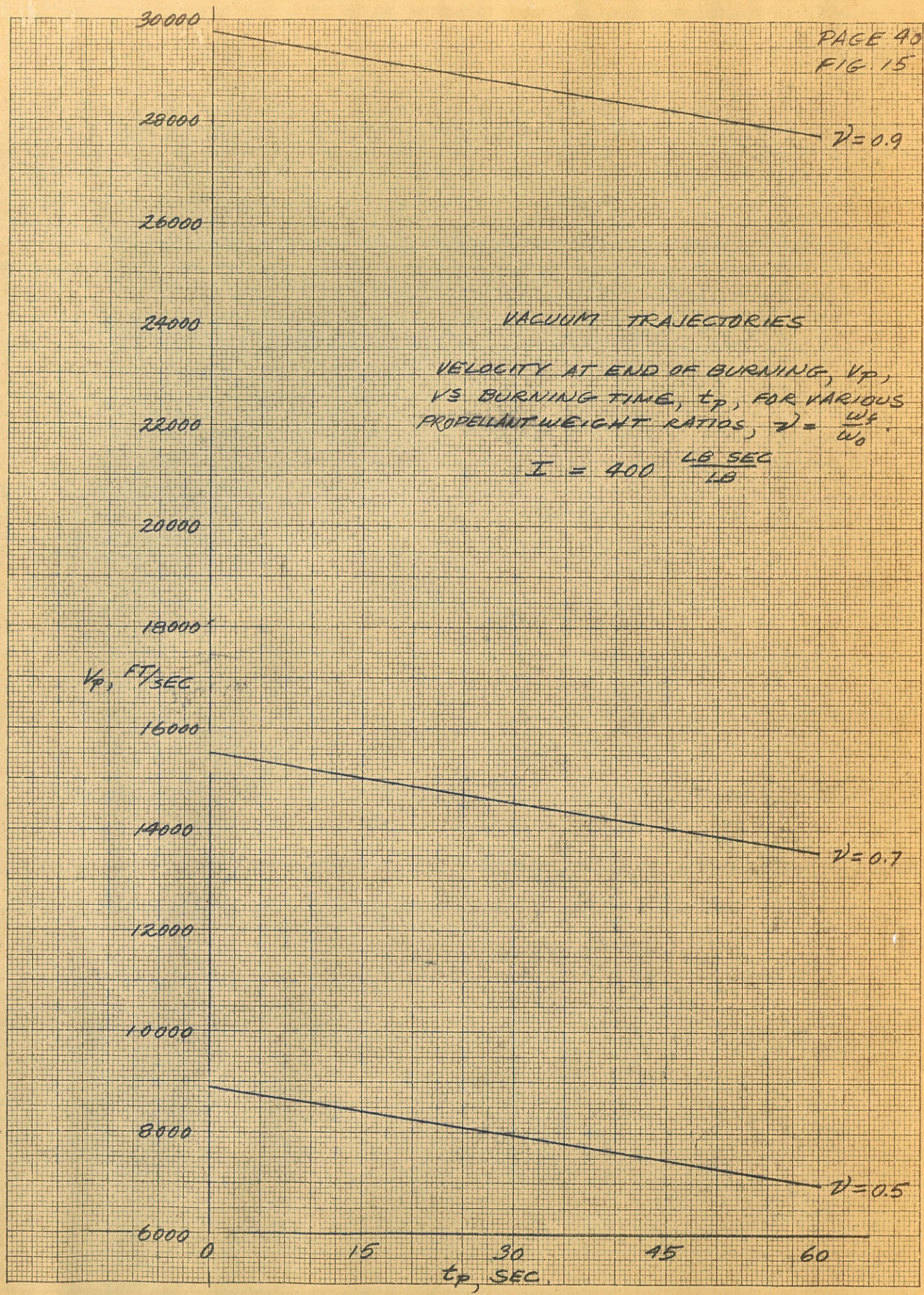

VACUUM TRAJECTORIES

VELOCITY AT END OF BURNING, V_p, VS BURNING TIME, t_p, FOR VARIOUS PROPELLANT WEIGHT RATIOS, $\nu = \frac{w_f}{w_0}$.

$I = 400 \frac{LB\ SEC}{LB}$

VACUUM TRAJECTORIES

ALTITUDE AT END OF BURNING, y_p VS BURNING TIME, t_p, FOR VARIOUS PROPELLANT WEIGHT RATIOS, $\nu = \frac{w_f}{w_0}$. $I = 150 \frac{LB\ SEC}{LB}$

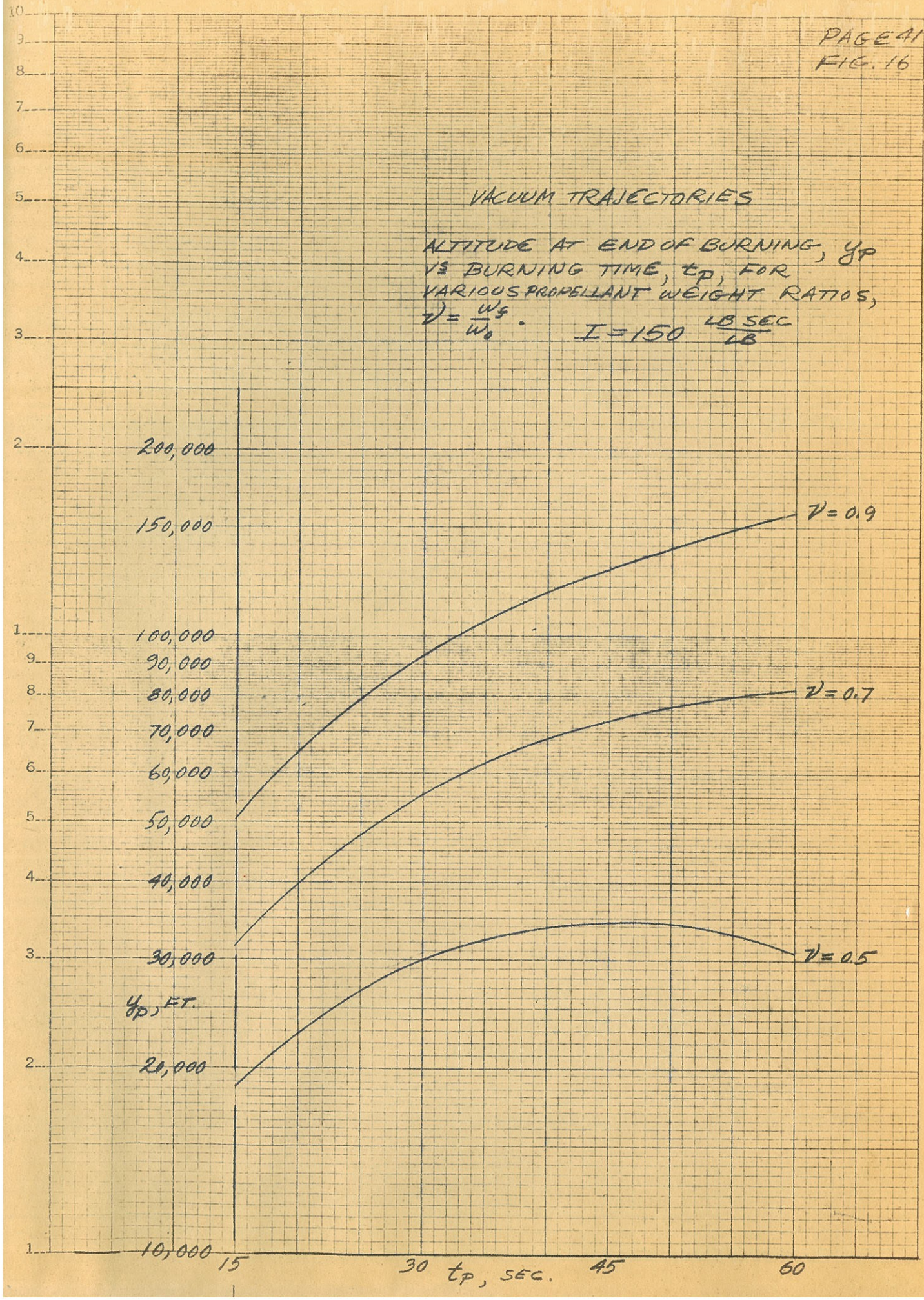

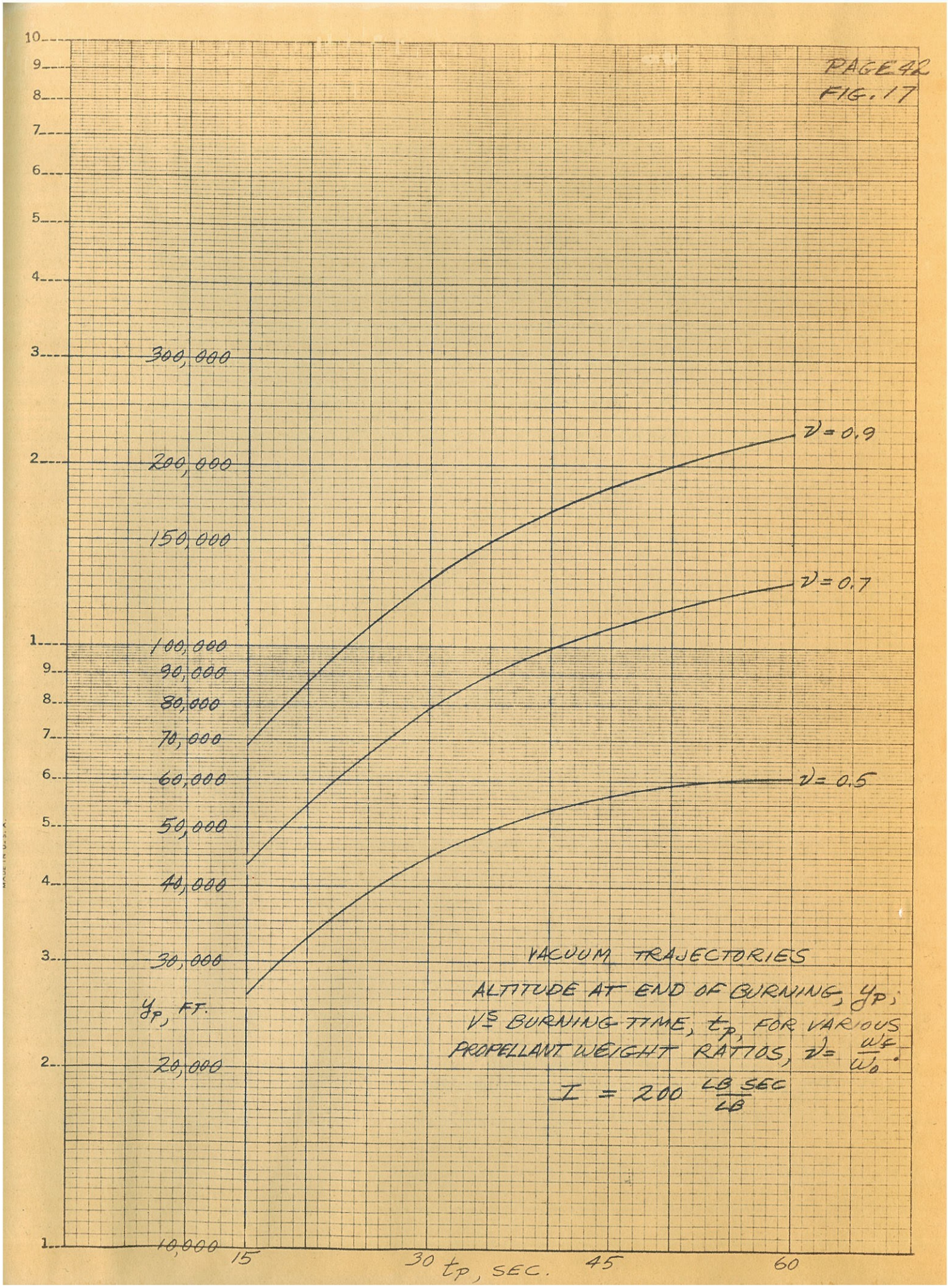

VACUUM TRAJECTORIES

ALTITUDE AT END OF BURNING, y_p; VS BURNING TIME, t_p, FOR VARIOUS PROPELLANT WEIGHT RATIOS, $\nu = \frac{w_f}{w_o}$.

$I = 200 \frac{LB\ SEC}{LB}$

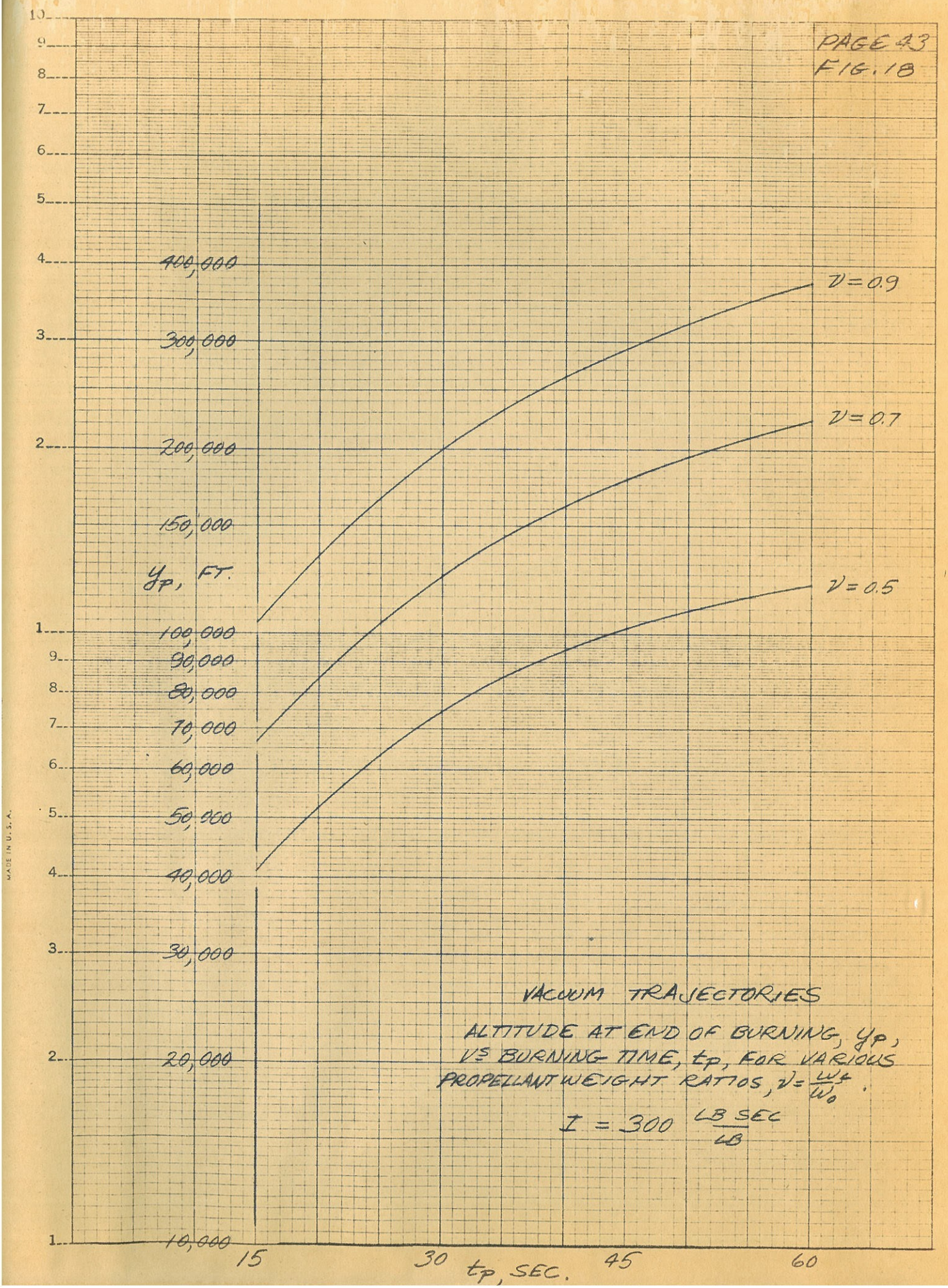

VACUUM TRAJECTORIES

ALTITUDE AT END OF BURNING, y_p, VS BURNING TIME, t_p, FOR VARIOUS PROPELLANT WEIGHT RATIOS, $\nu = \frac{W_f}{W_o}$.

$I = 300 \frac{LB\ SEC}{LB}$

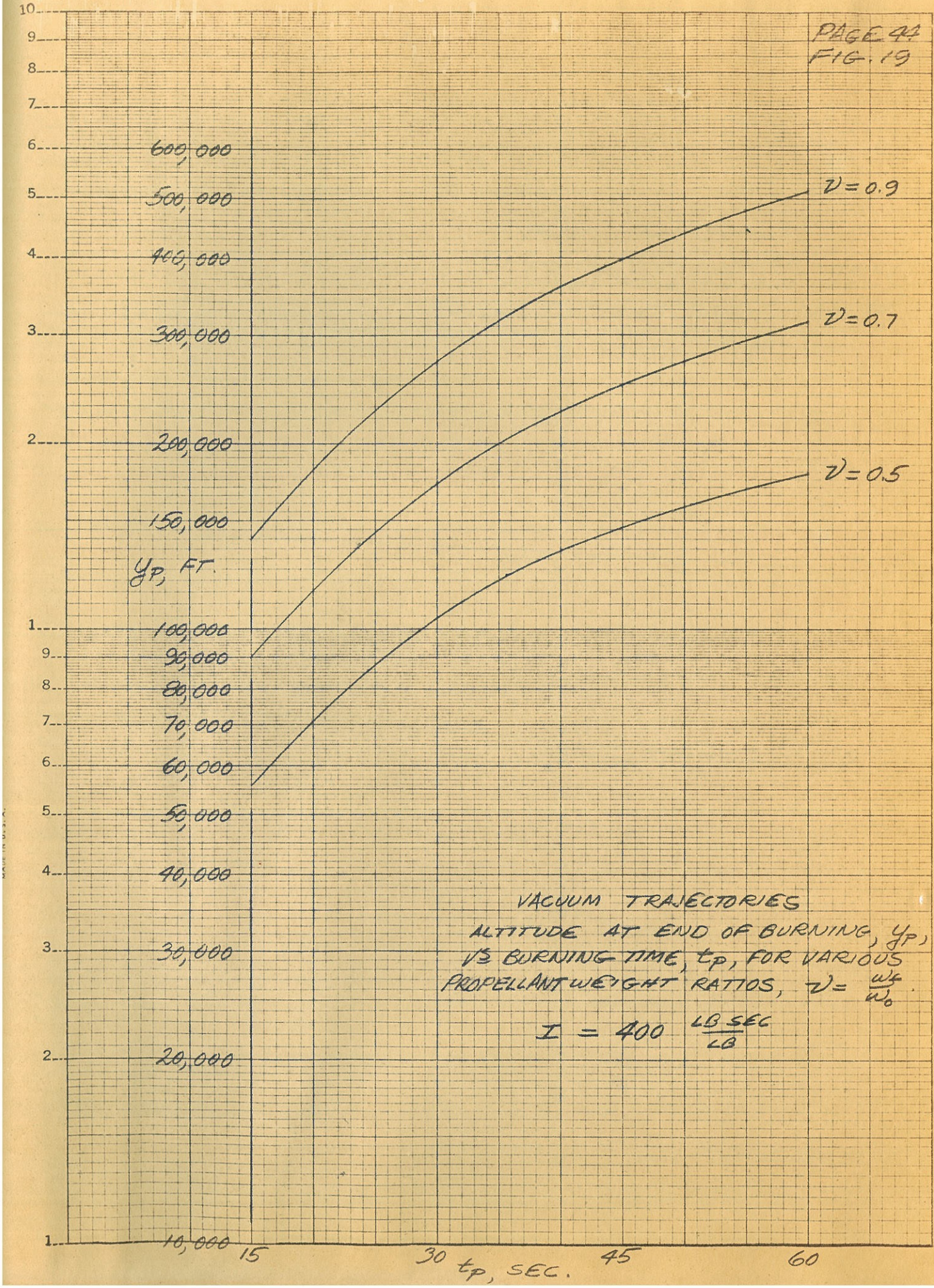

VACUUM TRAJECTORIES
ALTITUDE AT END OF BURNING, y_p,
VS BURNING TIME, t_p, FOR VARIOUS
PROPELLANT WEIGHT RATIOS, $v = \frac{w_f}{w_o}$.

$I = 400 \frac{LB\ SEC}{LB}$

PAGE 45
FIG. 20

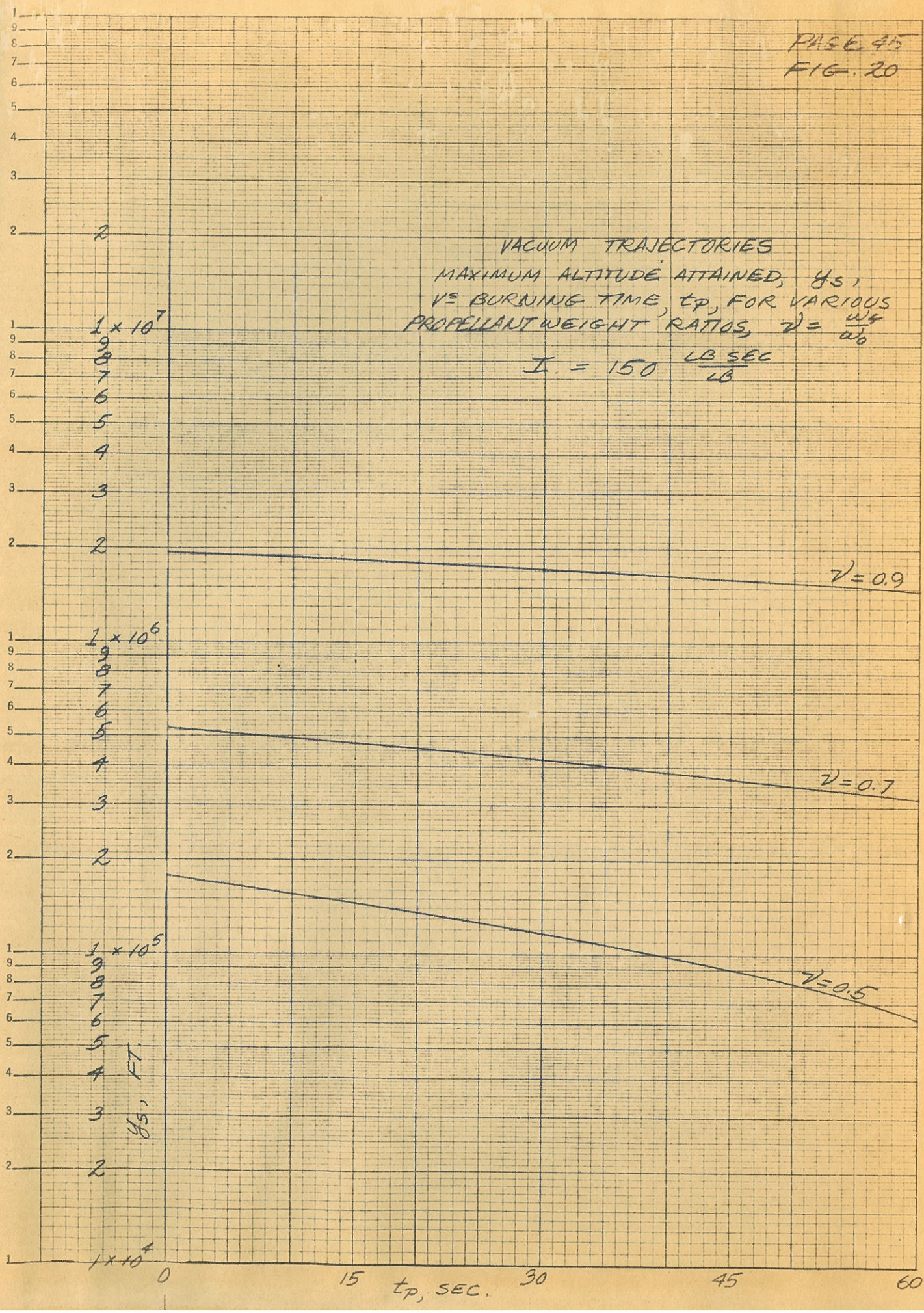

VACUUM TRAJECTORIES
MAXIMUM ALTITUDE ATTAINED, y_s,
VS BURNING TIME, t_p, FOR VARIOUS
PROPELLANT WEIGHT RATIOS, $\nu = \frac{W_f}{W_o}$

$I = 200 \frac{LB\ SEC}{LB}$

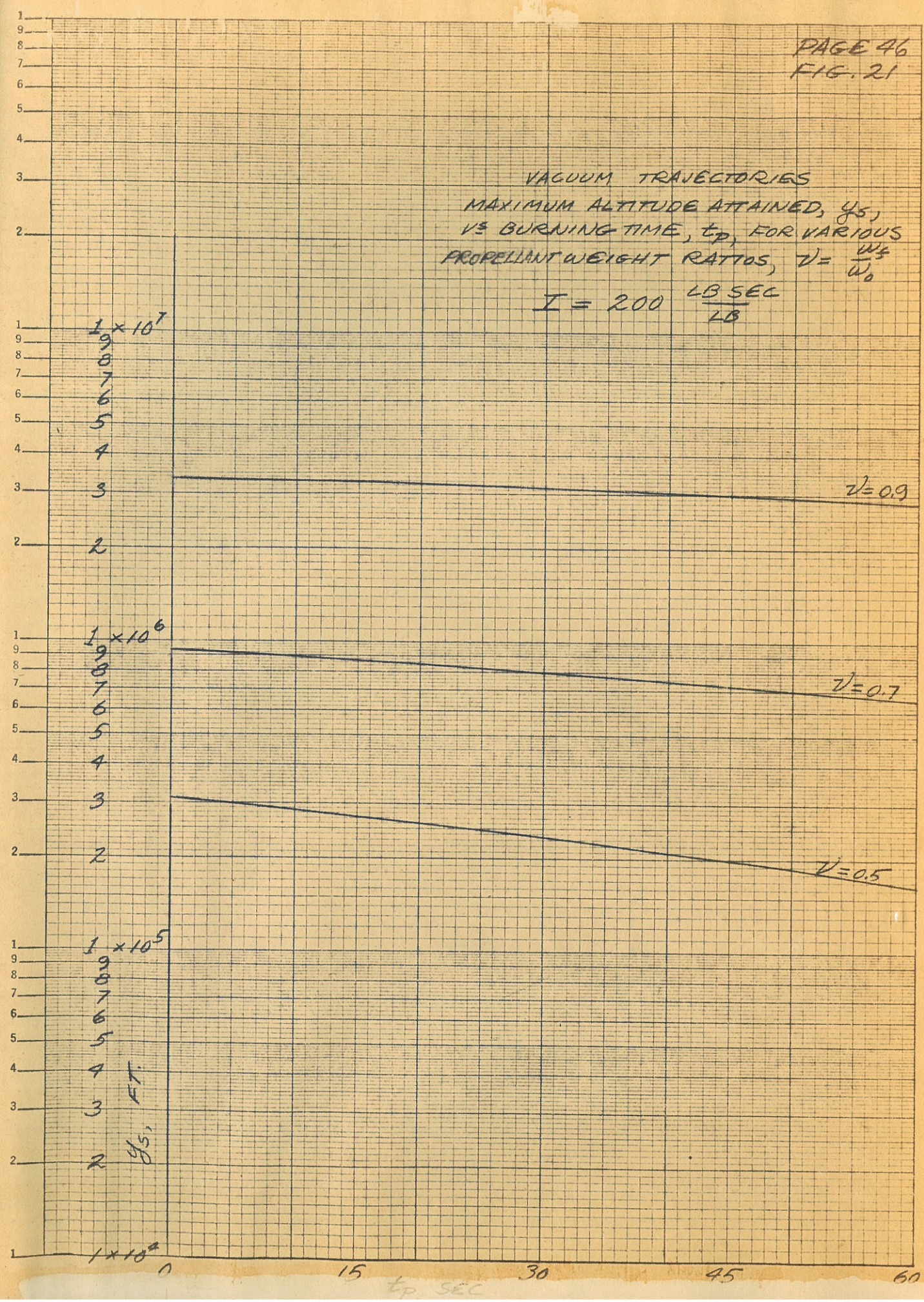

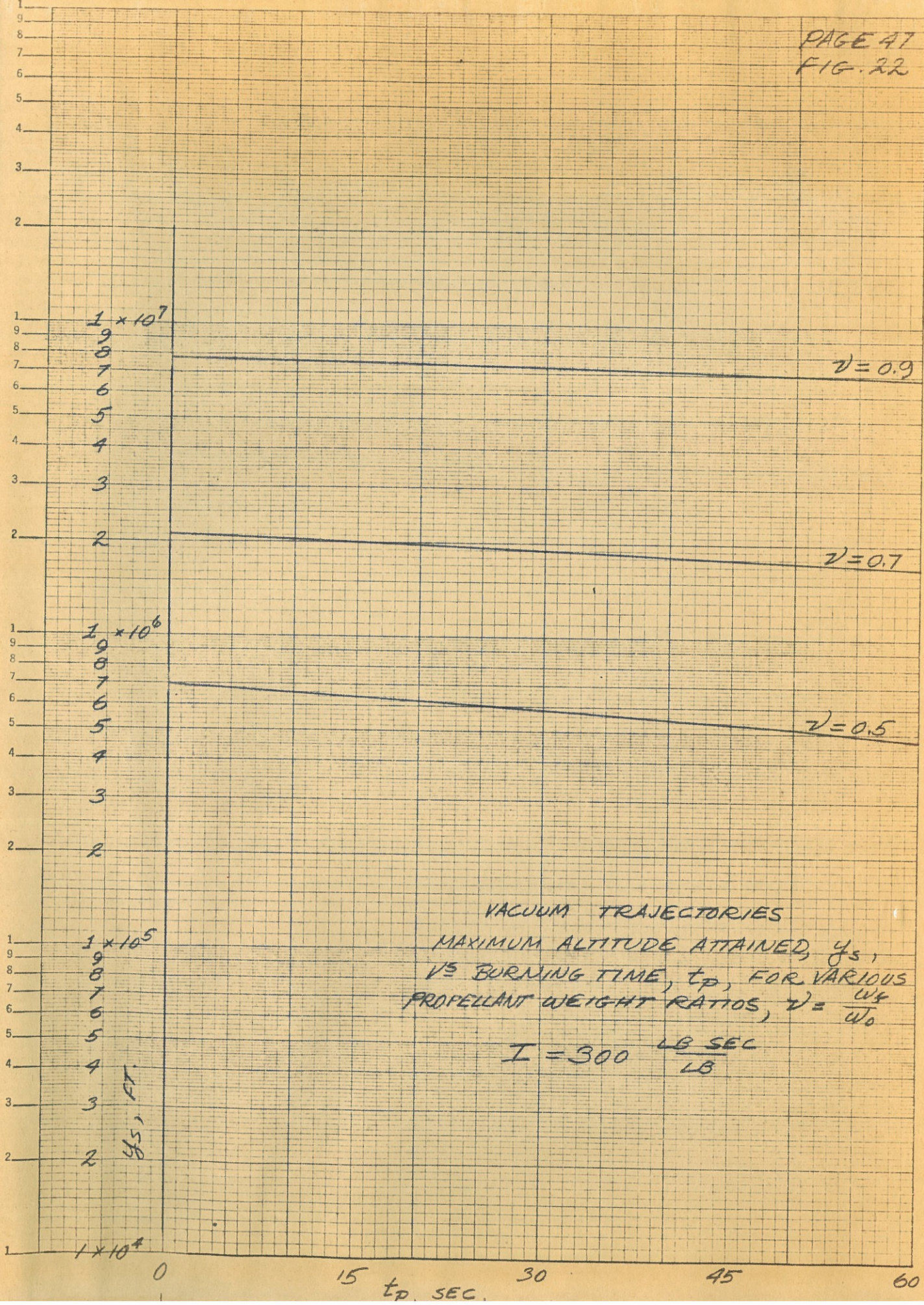

VACUUM TRAJECTORIES
MAXIMUM ALTITUDE ATTAINED, y_s,
VS BURNING TIME, t_p, FOR VARIOUS
PROPELLANT WEIGHT RATIOS, $\nu = \frac{W_f}{W_o}$

$I = 300 \frac{LB\ SEC}{LB}$

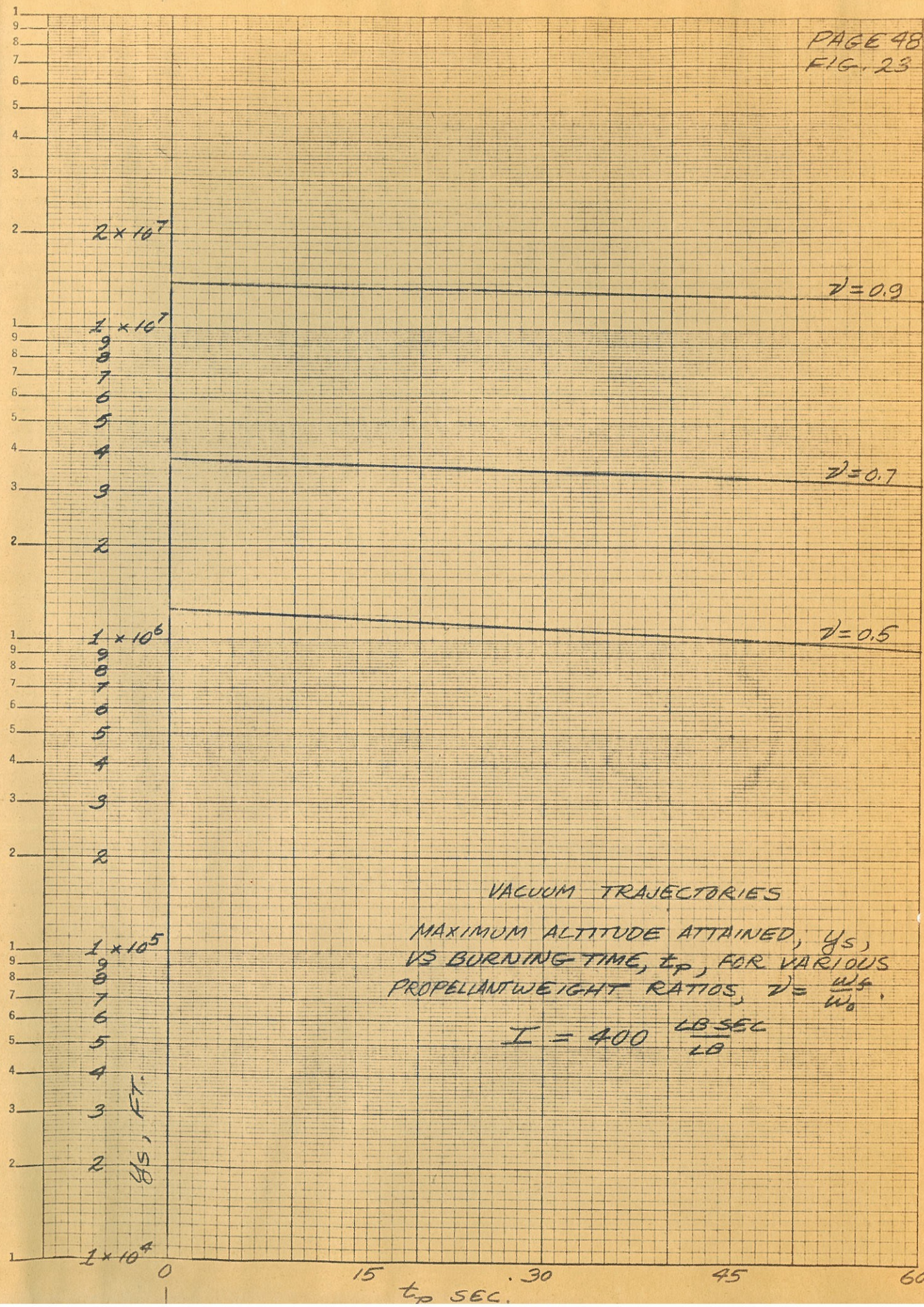

VACUUM TRAJECTORIES

MAXIMUM ALTITUDE ATTAINED, y_s, VS BURNING-TIME, t_p, FOR VARIOUS PROPELLANT WEIGHT RATIOS, $\nu = \frac{w_s}{w_0}$.

$I = 400 \frac{LB\,SEC}{LB}$

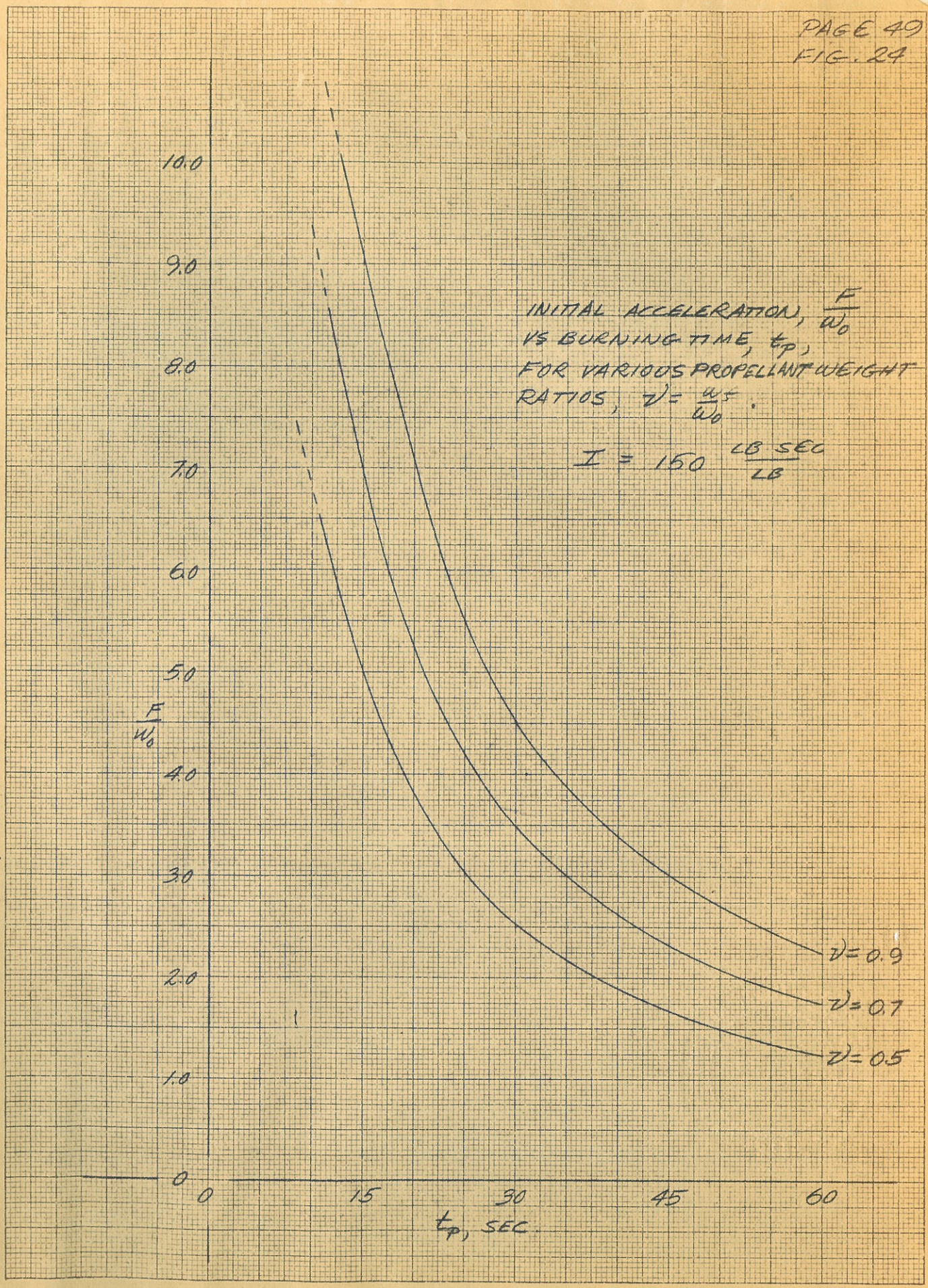
INITIAL ACCELERATION, $\frac{F}{W_0}$
VS BURNING TIME, t_p,
FOR VARIOUS PROPELLANT WEIGHT
RATIOS, $\nu = \frac{W_f}{W_0}$.
$I = 150 \frac{LB\ SEC}{LB}$
$\frac{F}{W_0}$
10.0
9.0
8.0
7.0
6.0
5.0
4.0
3.0
2.0
1.0
0
0
15
30
45
60
t_p, SEC.
$\nu = 0.9$
$\nu = 0.7$
$\nu = 0.5$

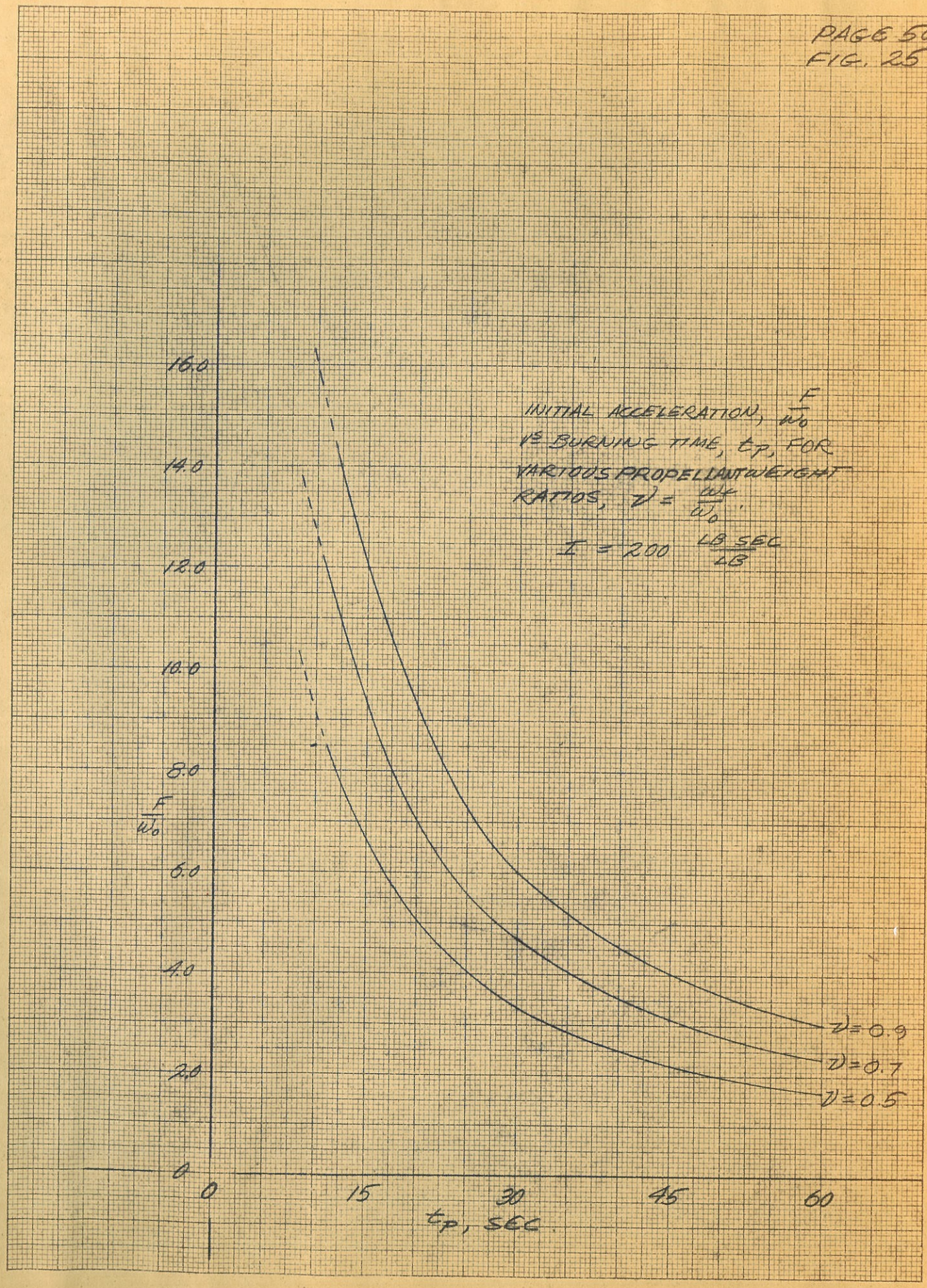
INITIAL ACCELERATION, $\frac{F}{w_0}$
VS BURNING TIME, t_p, FOR
VARIOUS PROPELLANT WEIGHT
RATIOS, $\nu = \frac{w_p}{w_0}$.
$I = 200 \frac{LB\ SEC}{LB}$
16.0
14.0
12.0
10.0
8.0
6.0
4.0
2.0
0
$\frac{F}{w_0}$
0
15
30
45
60
t_p, SEC
$\nu = 0.9$
$\nu = 0.7$
$\nu = 0.5$

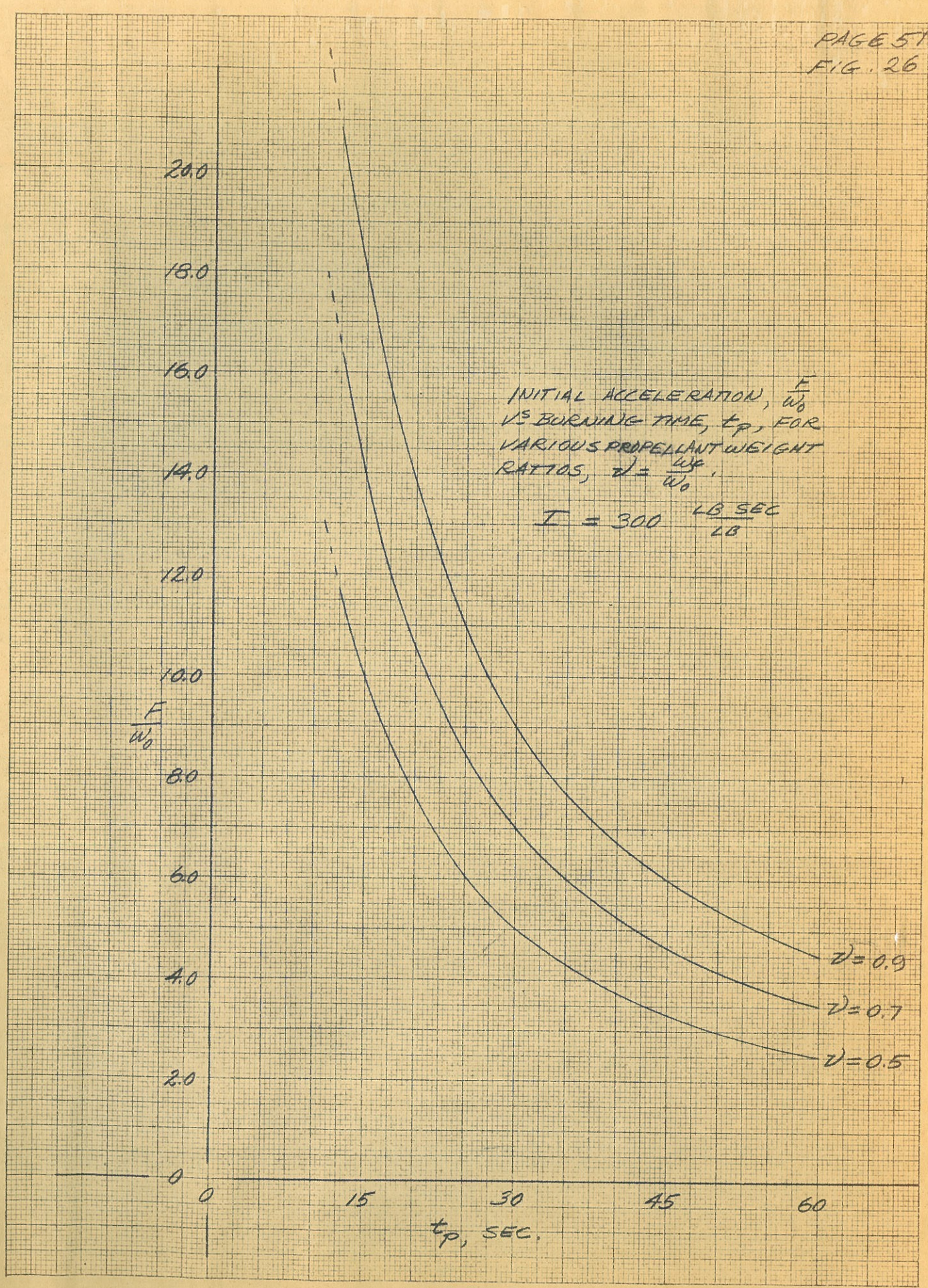
INITIAL ACCELERATION, $\frac{F}{W_0}$ VS BURNING TIME, t_p, FOR VARIOUS PROPELLANT WEIGHT RATIOS, $\nu = \frac{W_F}{W_0}$.
$I = 300 \frac{LB\ SEC}{LB}$
$\nu = 0.9$
$\nu = 0.7$
$\nu = 0.5$
$\frac{F}{W_0}$
20.0
18.0
16.0
14.0
12.0
10.0
8.0
6.0
4.0
2.0
0
0
15
30
45
60
t_p, SEC.

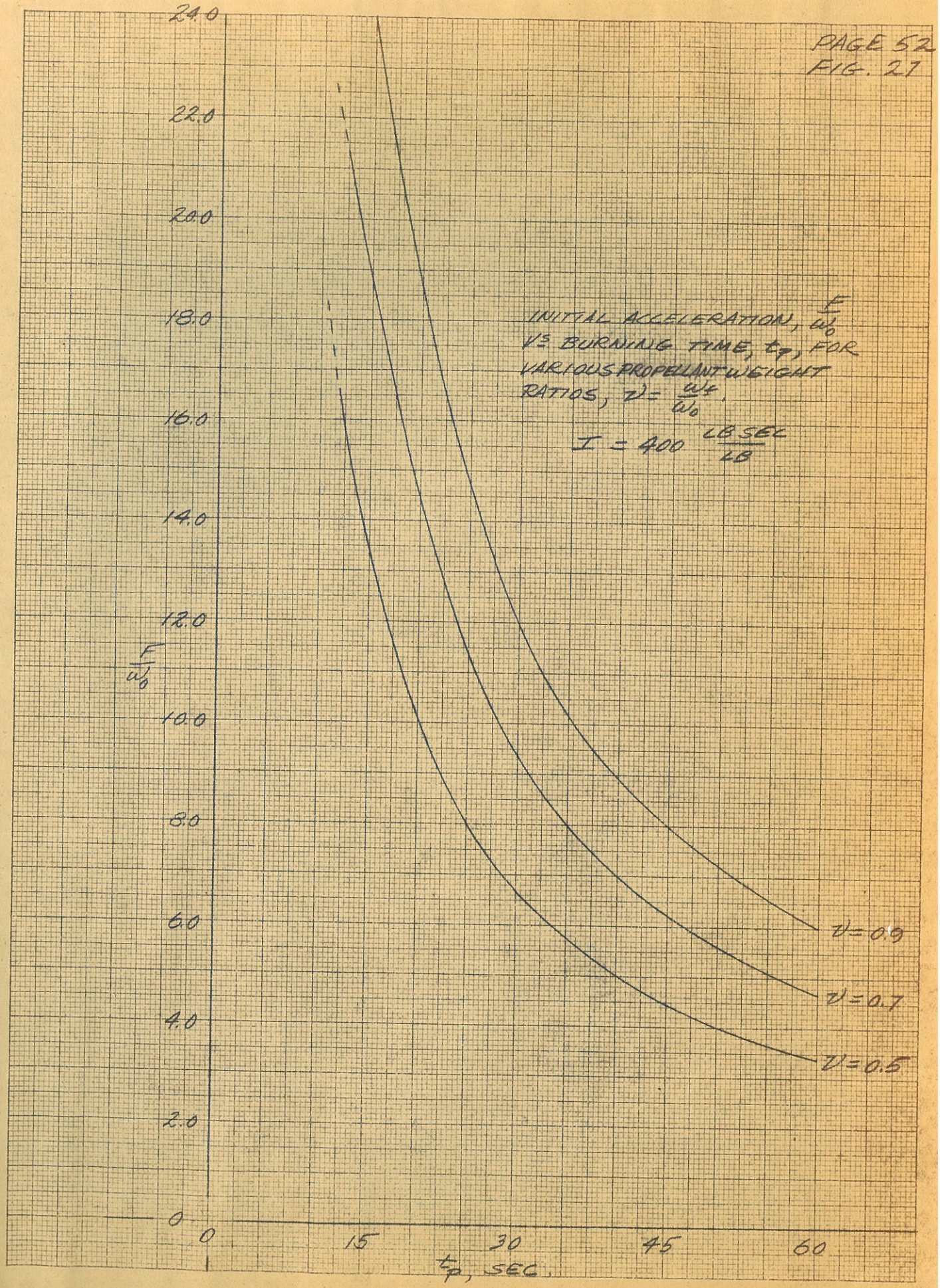
24.0
22.0
20.0
18.0
16.0
14.0
12.0
10.0
8.0
6.0
4.0
2.0
0
$\frac{F}{\omega_0}$
0
15
30
45
60
t_p, SEC.
INITIAL ACCELERATION, $\frac{F}{\omega_0}$ VS BURNING TIME, t_p, FOR VARIOUS PROPELLANT WEIGHT RATIOS, $\nu = \frac{\omega_f}{\omega_0}$.
$I = 400 \frac{LB\,SEC}{LB}$
$\nu = 0.9$
$\nu = 0.7$
$\nu = 0.5$

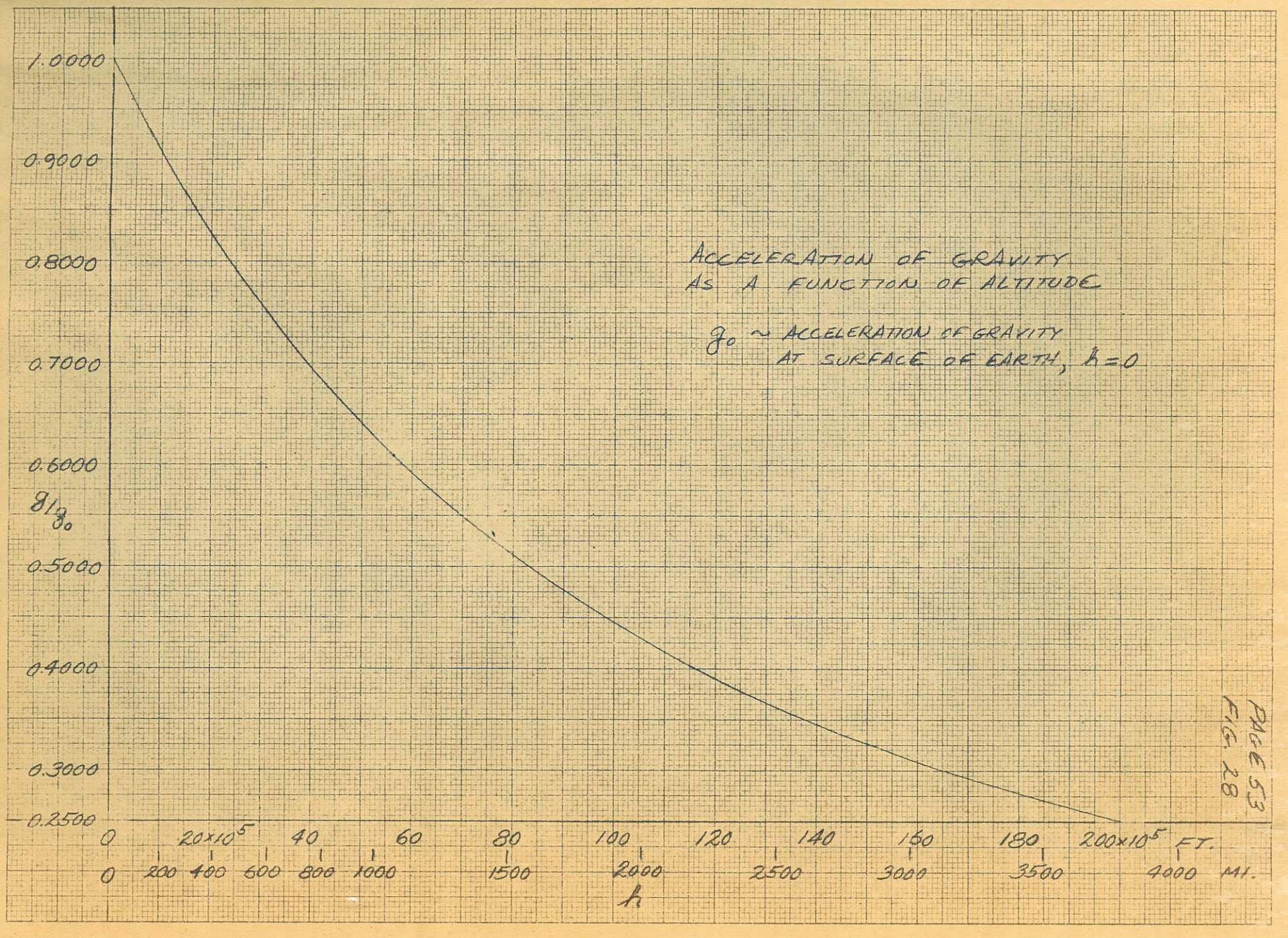

PAGE 53
FIG. 28

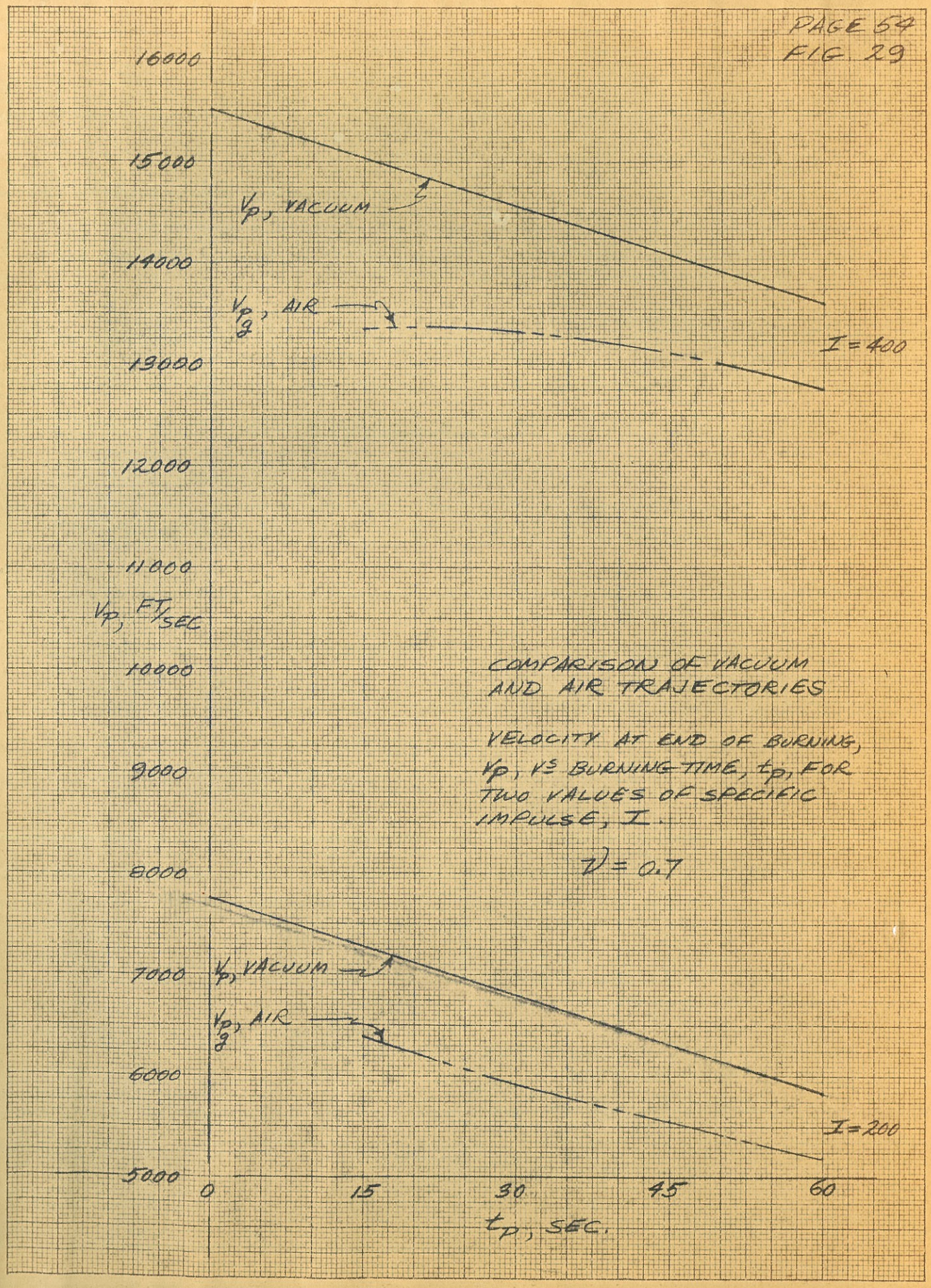

COMPARISON OF VACUUM AND AIR TRAJECTORIES

VELOCITY AT END OF BURNING, V_p, VS BURNING TIME, t_p, FOR TWO VALUES OF SPECIFIC IMPULSE, I.

$D = 0.7$

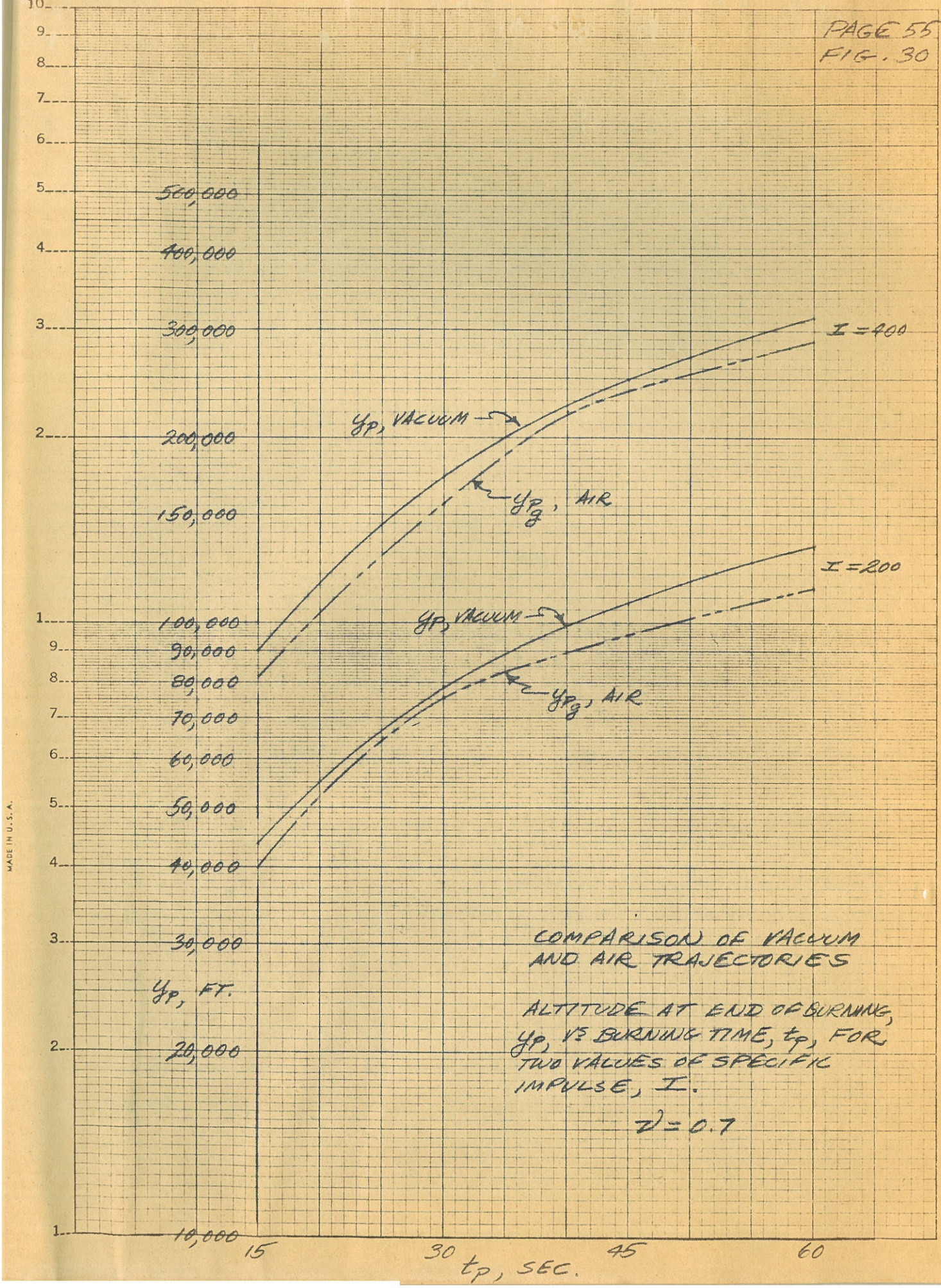

COMPARISON OF VACUUM AND AIR TRAJECTORIES

ALTITUDE AT END OF BURNING, y_p, VS BURNING TIME, t_p, FOR TWO VALUES OF SPECIFIC IMPULSE, I.

$\gamma = 0.7$

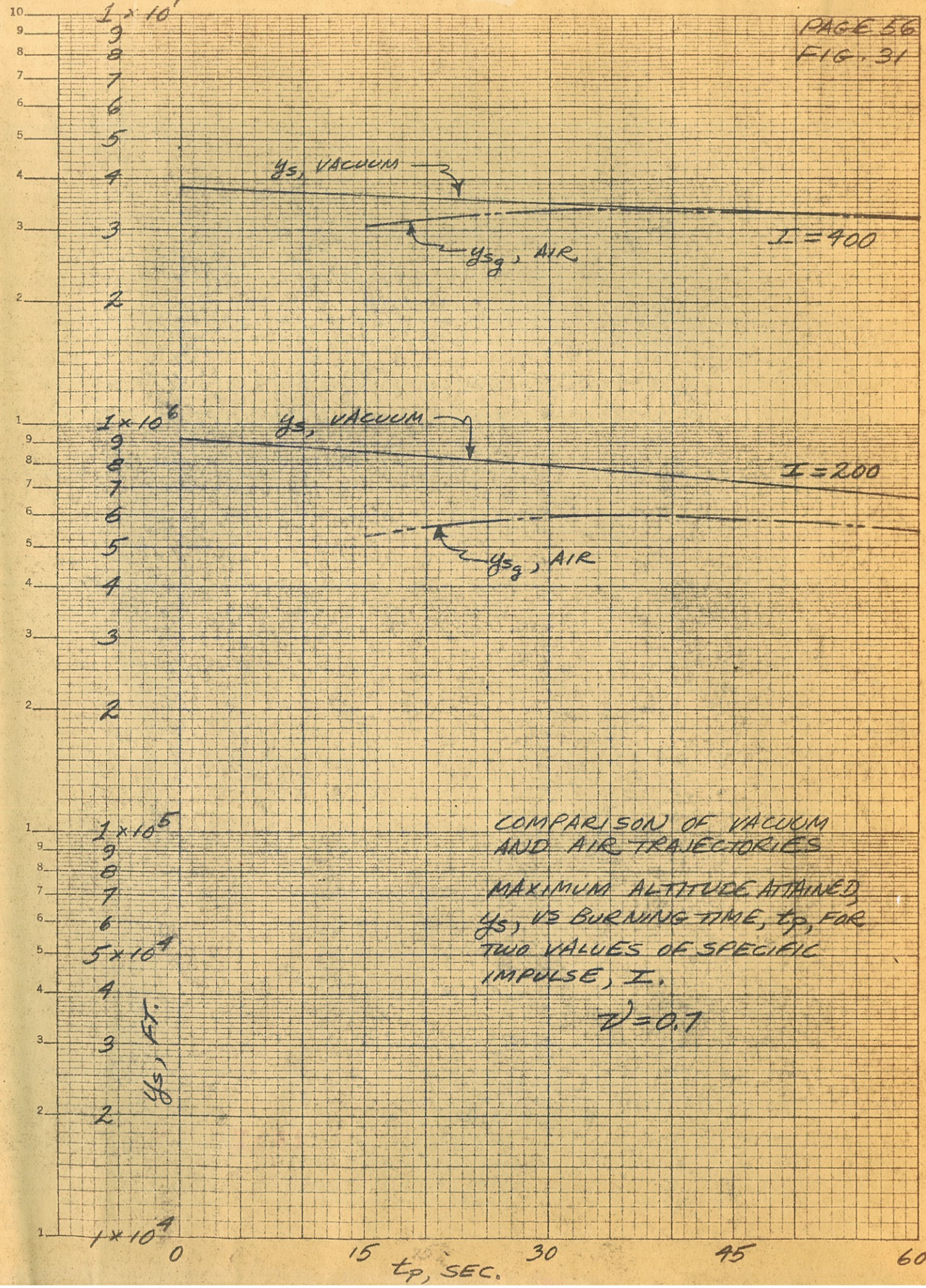

COMPARISON OF VACUUM AND AIR TRAJECTORIES

MAXIMUM ALTITUDE ATTAINED, y_s, VS BURNING TIME, t_p, FOR TWO VALUES OF SPECIFIC IMPULSE, I.

$\gamma = 0.7$